Table 2
The root mean square (rms) roughness of the modified glass surface topographies measured by AFM.

Surface condition	Cleaned glass	APTS	APTS-Fmoc-PL	APTS-PL	APTS-PL-MPC	UV (3 min)
Average RMS values (nm)	1.31 ± 0.34	2.59 ± 0.17	3.80 ± 0.12	4.58 ± 0.29	1.46 ± 0.14	5.31 ± 0.38

Scan size: 10 μm × 10 μm.

room temperature, rinsed with PBS three times, permeabilized by incubation with 0.5% Triton X-100 in PBS for 2 min, and rinsed with PBS three times. Then, nuclear staining was performed with 2 mg/mL DAPI for 2 min followed by rinsing with PBS three times. The sample dishes were filled with PBS and stained cells were observed under a fluorescence microscope.

2.12. Fluorescence microscopy

Fluorescence and phase-contrast images were acquired using a fluorescence microscope (IX 71, Olympus) with an objective lens (4×, 0.25-NA or 10×, 0.30-NA) and filter sets: U-MNIBA3 (470–495 nm exciter and 515–550 nm emitter) for FITC and calcein AM, U-MWIG3 (530–550 nm exciter and 575 nm emitter) for ethidium homodimer-1, and U-MNUA2 (360–370 nm exciter and 420–460 nm emitter) for DAPI. The images were recorded with a CCD camera (Retiga EXi, QIMAGING). Qcapture PRO Software was used to save the images in Microsoft Windows XP.

3. Results and discussion

3.1. Characterization of surface

3.1.1. Static water contact angle measurements

Each surface modification step was monitored by measuring the static water contact angle (Fig. 2a). Results showed that hydrophilicity of the surface changed significantly as the surface modification steps proceeded. When the bare glass surface was cleaned by 0.1 N NaOH, a 0° contact angle was obtained, indicating a highly hydrophilic surface. After treating this surface with APTS, the contact angle increased to 52°. Hydrophobicity increased when the Fmoc-photolabile linker was coupled to the APTS surface (APTS-Fmoc-PL) and the contact angle increased from 52° to 77°. After deprotection of the Fmoc group, contact angle decreased from 77° to 63° (APTS-PL). The glass surface became hydrophilic after the MPC polymer was grafted, resulting in a contact angle of 14°. These results suggest that an MPC polymer-modified surface (APTS-PL-MPC) was formed.

To change the surface from cell non-adhesive to adhesive, the MPC polymer should be eliminated from the surface by photocleavage. For this reason, UV illumination time was optimized using measurements of static water contact angle (Fig. 2b). The effect of UV illumination time on the contact angle of the MPC polymer-modified surface was monitored. Contact angle increased up to 3 min of UV irradiation time to 54°. After 3 min, the contact angle reached a plateau; no significant difference in contact angle occurred past that time. These results indicate that the MPC polymer had been completely removed from the glass surface after 3 min of UV irradiation. Thus, optimum UV illumination time was 3 min, and was used for further surface characterization experiments.

3.1.2. X-ray photoelectron spectroscopy (XPS)

The modified glass surfaces also were characterized by XPS. Table 1 shows the XPS composition of the modified glass surfaces. Only the grafting and elimination of MPC polymer on the MPC polymer-modified surface containing phosphorus could be confirmed by the XPS data. The MPC polymer-modified surface (APTS-PL-MPC) was compared with the APTS-PL and UV-irradiated surface. An XPS signal at 133 eV of the phosphorus 2p peak (Fig. 3b) was observed only on the MPC polymer-modified surface; no elemental P peak was observed on either APTS-PL (Fig. 3a) or the UV-irradiated surface (Fig. 3c) (Table 1). These results indicate that the MPC polymer is modified on the glass surface and effectively removed by UV illumination.

3.1.3. Atomic force microscopy (AFM)

AFM images were acquired from the modified glass surface; surface roughness (RMS) of the modified surfaces is shown in Table 2. Surface roughness changed as reaction time increased. When the cleaned bare glass surface was modified with APTS, RMS increased from 1.31 ± 0.34 nm to 2.59 ± 0.17 nm. After the Fmoc-photolabile linker was coupled to the APTS surface, the RMS value increased to 3.80 ± 0.12 nm. Cleavage of the Fmoc protecting group caused a increase in RMS to 4.58 ± 0.29 nm (Fig. 4a). Despite coupling of the MPC polymer (APTS-PL-MPC), the surface remained smooth (RMS = 1.46 ± 0.14 nm) as shown in Fig. 4b. These results indicate that the MPC polymer was grafted homogeneously on the surface. After cleavage of the MPC polymer, the surface roughness increased from 1.46 ± 0.14 nm to 5.31 ± 0.38 nm (Fig. 4c).

3.2. Protein adsorption

The amount of non-specific adsorption of two different types of proteins (BSA and fibronectin) was investigated on a modified glass

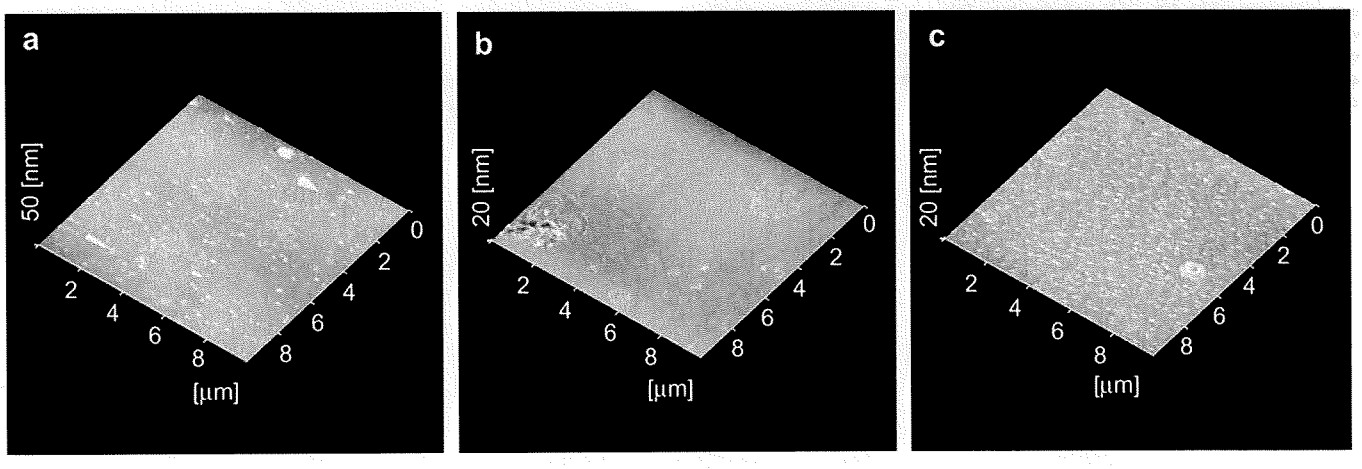

Fig. 4. AFM images of the modified surface (10 μm × 10 μm). (a) APTS-PL, (b) APTS-PL-MPC, (c) UV-irradiated surface.

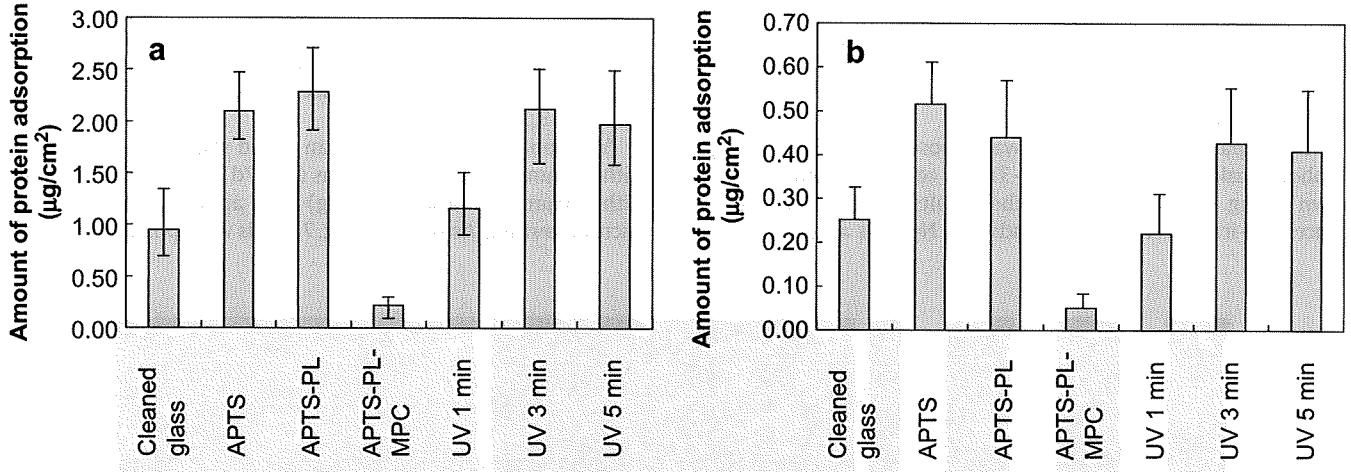

Fig. 5. The amounts of proteins absorbed on modified glass substrate. (a) BSA, (b) fibronectin. The error bars represent standard deviations.

substrate, as shown in Fig. 5. BSA is used as a blocking agent and fibronectin is an ECM protein that promotes cell attachment. Fibronectin interacts with cell integrins, which play a pivotal role in cell attachment. Non-specific adsorption of fibronectin on the modified surfaces should reveal related properties for selective cell micropatterning. The amounts of adsorbed BSA and fibronectin on each APTS surface were 2.10 μg/cm^2 and 0.52 μg/cm^2, respectively. On the APTS-PL surface, 2.28 μg/cm^2 of BSA and 0.36 μg/cm^2 of fibronectin were adsorbed, respectively. For an MPC polymer-modified surface, 0.22 μg/cm^2 of BSA and 0.05 μg/cm^2 of fibronectin attached. Compared with APTS, the amount of non-specific protein adsorption on the MPC polymer-modified (APTS-PL-MPC) surface decreased to 10–14%, indicating that the MPC polymer-modified surface effectively suppressed non-specific protein adsorption. The amount of BSA (0.22 μg/cm^2) on the MPC polymer surface was similar to that reported previously [35]. In contrast, as the amount of MPC polymer removed was increased by UV illumination, the amount of adsorbed proteins on the surface also increased. After 1 min of UV irradiation, 1.16 μg/cm^2 of BSA and 0.22 μg/cm^2 of fibronectin were attached; the amount of adsorbed proteins increased to 2.12 μg/cm^2 of BSA and 0.43 μg/cm^2 of fibronectin upon 3 min of irradiation. Upon 5 min of UV illumination, 1.97 μg/cm^2 of BSA and 0.41 μg/cm^2 of fibronectin were adsorbed, which did not change appreciably from the absorption amounts seen at 3 min of UV illumination. Non-specific protein adsorption generally tends toward increased adsorption with decreased wettability [36,37]. The trends observed in the experiments conducted for this study were similar to those of the hydrophilicity experiments shown in Fig. 2.

3.3. Cell attachment

The number of MC-3T3 E1 cells attached on each modified surface is shown in Fig. 6. After silanization (APTS surface) of the cleaned bare glass surface, the number of attached cell increased from 113 to 167 cells. The number of cells adhered on the APTS-PL surface was 236. However, no cells adhered to the MPC polymer-modified surface (APTS-PL-MPC), which was expected. When the MPC polymer was removed by 3 min of UV illumination, cell adherence was re-established at 212 cells. These results were in agreement with the surface wettability (Fig. 2) and the surface roughness results (Table 2), which confirmed that cell attachment can be controlled by photochemical reactions. Furthermore, control experiments were carried out without introducing PL. MPC polymer was grafted directly on amino-silanized surface (APTS-MPC), and UV was exposed to APTS-MPC polymer-modified surface for 3 min. On these two surfaces (APTS-MPC, UV-irradiated surface), the cell attachment test was estimated as above. No attached cell was found in both surfaces. These results indicate that MPC polymer was eliminated by photochemical reaction.

Surface properties, such as surface chemistry [38], functional group [39], roughness [40], charge [41], and wettability [33,34] are closely related to cell attachment. In the systems described here, the wettability, roughness and nature of the surface terminal groups were considered together. As seen in Fig. 6, the cell adhesiveness increased according to the increase in the surface wettability and the surface roughness. When the modified surface was exposed to UV light, aromatic terminal groups remained on the surface [28,29]. Many studies about the effects of surface functional groups on cell attachment have been published. However, few reports exist on the role of aromatic terminal groups on surface characteristics. Studies have reported that an aromatic ring close to an ionizable group increased cell attachment [42] and aromatic terminal groups acted as platforms for cell adherence [43]. Aromatic terminal groups might also have an effect on localization of cells on some surfaces.

3.4. Micropatterning of biological samples

Biological micropatterning was performed using a photochemical reaction strategy. A photomask with 200-μm wide stripes with black 300-μm separations (Fig. 7a) was used.

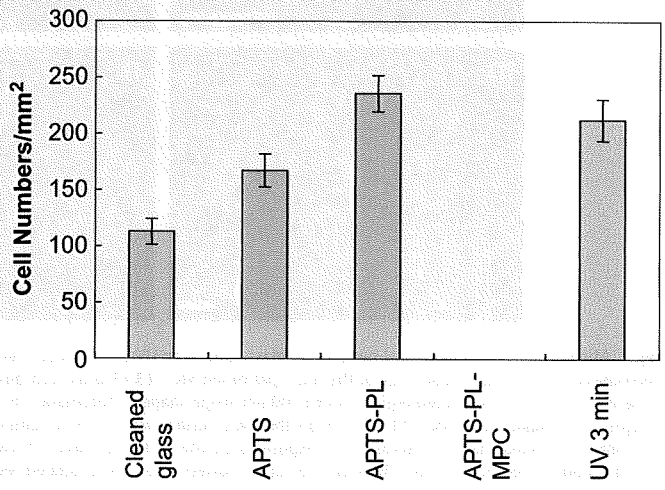

Fig. 6. The number of MC-3T3 E1 cells attached on modified glass substrate (cell number/mm^2). The error bars represent standard deviations.

Protein adsorption to a patterned surface was observed using FITC-BSA florescence microscopy, as shown in Fig. 7b. BSA was localized to the UV-irradiated area where the MPC had been removed and a striped pattern formed that matched the stripes of the photomask (Fig. 7a).

After preparing each surface, it was exposed to UV light through the photomask. The results for MC-3T3 E1 cell micropatterning are shown in Fig. 7c. This indicates the results of cells cultured on surfaces UV-irradiated and not irradiated. No cells attached to the MPC polymer-modified surface; however, cells attached selectively on the UV-irradiated region. The size of the micropatterned cells coincided with the area exposed by the photomask. Cells tended to attach to a hydrophobic surface, which agrees with previous studies [33,34].

Additionally, photomasks of an round shape 50 μm in diameter with 250 μm, 150 μm separations (Fig. 7d), and 30 μm in diameter with 150 μm separations (Fig. 7g) were applied to MC-3T3 E1 cell micropatterning. As shown in Fig. 7e, cells were positioned at 50-μm

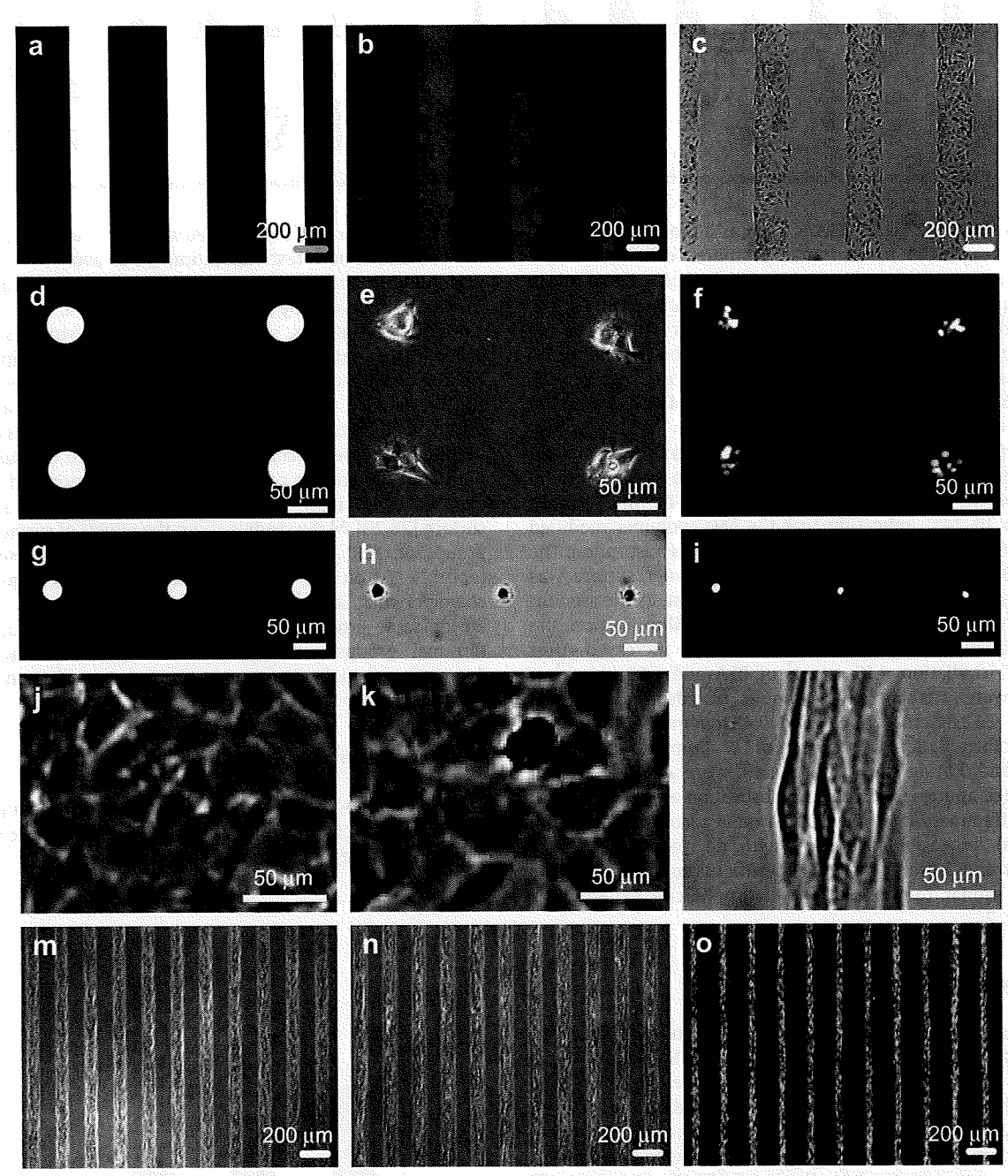

Fig. 7. Micropatterning of biological samples on glass surface by UV illumination. Width 200 μm stripe shaped photomask (a–c), diameter 50 μm (d–f), 30 μm (g–i) round shaped photomasks were used, morphology of the micropatterned MC-3T3 E1 cells according to pattern size (j–l). Stability of the micropatterned MC-3T3 E1 cells on the glass modified surface (m–o). (a) UV-irradiated region (width 200 μm stripe shaped photomask). (b) Fluorescence images of micropatterned BSA adsorbed on the glass surface. (c) Phase-contrast images of micropatterned MC-3T3 E1 cells on the glass surface after 12 h of culture. (d) UV-irradiated region (diameter 50 μm round shaped photomask). (e) MC-3T3 E1 cell attachment to round shaped patterns on UV exposed area after 1 day of culture. (f) Fluorescence images of (e), nucleus were stained with DAPI. (g) UV-irradiated region (diameter 30 μm round shaped photomask). (h) Single cell array-patterned on UV-irradiated region after 4 h of incubation. (i) Fluorescence images (h), stained with DAPI. Magnified phase-contrast images of MC-3T3 E1 cells attached on UV-illuminated surface (j–l, captured size: 140 μm × 100 μm). (j) Without a photomask, (k) width 200 μm, (l) width 70 μm stripe shaped photomask. Phase-contrast images of MC-3T3 E1 cells on long-term cultures (m) 1 day of culture, (n) 35 days of culture, (o) Two color fluorescence images of (n) after treating with LIVE/DEAD viability/cytotoxicity Kit.

cell adhesive spots, which is comparable to the size of the photomask. However, in this case, the pattern size was wide enough to produce a single cell level pattern (Fig. 7f). To realize the single cell size level patterning, a photomask of 30-μm round spots was used. After 4 h of incubation, single cells were attached in an array on the patterned surface (Fig. 7h). To determine whether single cells were adhered in one spot, the nuclei were stained with DAPI before cell proliferation. Only one nucleus was observed in each pattern (Fig. 7i); among all of the patterns, about 10% of the micropatterns contained two cells. These results indicate that the present technique regulates single cell level.

Morphology of the micropatterned MC-3T3 E1 cells were observed by pattern size. During UV illumination, three different conditions were used: without a photomask, a photomask with a width of 200 μm, and a photomask with a width of 70 μm in a stripe shape. Localization of cells was done as described above. After 1 day of culture, adhered cells were detected by microscopy. A part of each image was magnified to the same size (140 μm × 100 μm) and cell morphology was compared. Additionally, aspect ratio (smaller width-to-length aspect ratios) of each cell was estimated (40 cells were averaged) from the obtained images in three different conditions.

For the experiments without a photomask and that with a 200-μm stripe photomask, no tendency of a uniform spread of cells was observed (Fig. 7j). Cells attached randomly on the UV-irradiated surface without any directionality. In the case of the 200-μm stripe photomask, most of the cells have no specific directionality (Fig. 7k), except for the cells that adhered at the edge of the pattern. This interesting phenomenon was further observed when using the photomask with a 70-μm stripe. Vertical directionality of the patterned cells was observed, in the same direction as the stripe of the photomask (Fig. 7l).

Furthermore, the aspect ratio of cell morphology; length divided by width, from different patterns was compared. The aspect ratio of three different conditions (without a photomask, a photomask with a width of 200 μm, and a photomask with a width of 70 μm in a stripe shape) were 1.70 ± 0.60, 1.32 ± 0.19, and 7.56 ± 0.60. High aspect ratio was obtained only width 70-μm cell pattern, because the observed uniform directionality of the patterned cells. When paying attention only to the cells at the edge of 200-μm pattern, a uniform spread of cell with high aspect ratio (5.97 ± 1.22) could be calculated, cells at this region were kept from spreading outside of the pattern and instead elongated. These results show that uniform directionality of cells can be achieved by choosing an appropriate pattern size.

3.5. Stability of the micropatterned cells in long-term cultures

To test long-term cultures for cell-based drug screening and fundamental cellular studies after cell micropatterning, the non-adhesive surface should contain the stable pattern. Therefore, micropatterning of MC-3T3 E1 cells (with a 100-μm stripe pattern) was performed on cover slide glass. MC-3T3 E1 cells maintained the patterns from day 1 to day 35 (Fig. 7m and n) without allowing outgrowth of the patterned cells. Furthermore, the viability of micropatterned MC-3T3 E1 cells was checked after 5 weeks of culturing (LIVE/DEAD Viability/Cytotoxicity Kit, Molecular Probes). Only live cells were detected by fluorescence microscopy (Fig. 7o). The micropatterned cells maintained not only pattern stability but also cell viability for 5 weeks of culturing.

Our data demonstrate that MPC polymer-modified surfaces maintain resistance to cells after 5 weeks of culturing, indicating that the non-adhesive properties of MPC polymer do not decrease under cell-culture conditions. The area of MPC polymer-modified surface area using this successive surface modification method was stable enough to inhibit the cell attachment on the surface during 5 weeks of culturing. Cells can synthesize and secrete their own ECM proteins for migration [44]. However, those ECM proteins were not adsorbed on the non-UV-irradiated area where the MPC polymer was modified.

4. Conclusions

A surface-treatment method using an MPC polymer and photolabile linker was developed for regulating cell attachment to a glass surface. UV illumination allowed the efficient removal of the MPC polymer, and control of cell attachment was achieved even to the single cell level. Results confirmed that the cells possessed a strong affinity to aromatic compounds that remained on the moderately hydrophobic surface after cleavage of the MPC polymer. Cell micropatterning of MC-3T3 E1 cells was achieved and maintained for 5 weeks. This method allows to control the spatial distribution of numbers of cells into specific shapes and sizes, with a stable location and distance between cells over long-term culturing. This technique can be applied to develop techniques for fundamental cell-based studies that analyze cell signaling and detect two different types of cell interactions.

References

[1] Lee JY, Jones C, Zern MA, Revzin A. Analysis of local tissue-specific gene expression in cellular micropatterns. Anal Chem 2006;78:8305–12.
[2] Yang J, Yamato M, Okano T. Cell-sheet engineering using intelligent surfaces. MRS Bull 2005;30:189–93.
[3] Jiang XY, Bruzewicz DA, Wong AP, Piel M, Whitesides GM. Directing cell migration with asymmetric micropatterns. Proc Natl Acad Sci U S A 2005;102:975–8.
[4] Kapur R, Giuliano KA, Campana M, Adams T, Olson K, Jung D, et al. Streamlining the drug discovery process by integrating miniaturization, high throughput screening, high content screening, and automation on the cellchip system. Biomed Microdevices 1999;2:99–109.
[5] McBeath R, Pirone DM, Nelson CM, Bhadriraju K, Chen CS. Cell shape, cytoskeletal tension, and rhoA regulate stem cell lineage commitment. Dev Cell 2004;6:483–95.
[6] Iwasaki Y, Ishihara K. Phosphorylcholine-containing polymers for biomedical applications. Anal Bioanal Chem 2005;381:534–46.
[7] Ishihara K, Ueda T, Nakabayashi N. Preparation of phospholipids polymers and their properties as polymer hydrogel membrane. Polym J 1990;22:355–60.
[8] Ishihara K, Aragaki R, Ueda T, Watanabe A, Nakabayashi N. Reduced thrombogenicity of polymers having phospholipid polar group. J Biomed Mater Res 1990;24:1069–77.
[9] Neff JA, Tresco PA, Caldwell KD. Surface modification for controlled studies of cell–ligand interactions. Biomaterials 1999;20:2377–93.
[10] Bearinger JP, Castner DG, Golledge SL, Rezania A, Hubchak S, Healy KE. P (AAm-*co*-EG) interpenetrating polymer networks grafted to oxide surfaces: surface characterization, protein adsorption and cell detachment studies. Langmuir 1997;13:5175–83.
[11] Chen CS, Mrksich M, Huang S, Whitesides GM. Geometric control of cell life and death. Science 1997;276:1425–8.
[12] Kunar A, Whitesides GM. Features of gold having micrometer to centimeter dimensions can be formed through a combination of stamping with an elastomeric stamp and alkanethiol ink followed by chemical etching. Appl Phys Lett 1993;63:2002–20.
[13] Bernard A, Delamarche E, Schmid H, Michel B, Bosshard HR, Biebuyck H. Printing patterns of proteins. Langmuir 1998;14:2225–9.
[14] McFarland CD, Thomas CH, DeFilippis C, Steele JG, Healy KE. Protein adsorption and cell attachment to patterned surfaces. J Biomed Mater Res 2000;49:200–10.
[15] Ward JH, Bashir R, Peppas NA. Micropatterning of biomedical polymer surfaces by novel UV polymerization techniques. J Biomed Mater Res 2001;56:351–60.
[16] Liu VA, Bhatia SN. Three-dimensional photopatterning of hydrogels containing living cells. Biomed Microdevices 2002;4:257–66.
[17] Luo Y, Shoichet MS. A photolabile hydrogel for guided three-dimensional cell growth and migration. Nat Mater 2004;3:249–53.
[18] Fink J, Thery M, Azioune A, Dupont R, Chatelain F, Bornens M, et al. Comparative study and improvement of current cell micro-patterning techniques. Lab Chip 2007;7:672–80.
[19] Konno T, Hasuda H, Ishihara K, Ito Y. Photo-immobilization of a phospholipid polymer for surface modification. Biomaterials 2005;26:1381–8.
[20] Sun J, Graeter SV, Yu L, Duan S, Spatz JP, Ding J. Technique of surface modification of a cell-adhesion-available inorganic microarray. Biomacromolecules 2008;9:2569–72.
[21] Kaji H, Kawashima T, Nishizawa M. Patterning cellular motility using an electrochemical technique and a geometrically confined environment. Langmuir 2006;22:10784–7.

[22] Yeo WS, Yousaf MN, Mrksich M. Dynamic interfaces between cells and surfaces: electroactive substrates that sequentially release and attach cells. J Am Chem Soc 2003;125:14994–5.
[23] Nakanishi J, Kikuchi Y, Takarada T, Yamaguchi K, Maeda M. Photoactivation of a substrate for cell adhesion under standard fluorescence microscopes. J Am Chem Soc 2004;126:16314–5.
[24] Kaji H, Sekine S, Hashimoto M, Kawashima T, Nishizawa M. Stepwise formation of patterned cell co-cultures in silicone tubing. Biotech Bioeng 2007;98:919–25.
[25] Thomas CH, Lhoets JB, Castner DG, McFarland CD, Healy KE. Surfaces designed to control the projected area and shape of individual cells. J Biomech Eng 1999;121:40–8.
[26] Veuseh M, Zhang M. Effect of silicon oxidation on long-term cell selectivity of cell-patterned Au/SiO_2 platforms. J Am Chem Soc 2006;128:1197–203.
[27] Lussi JW, Falconnet D, Hubbell JA, Textor M, Csucs G. Pattern stability under cell culture conditions-A comparative study of patterning methods based on PLL-g-PEG background passivation. Biomaterials 2006;27:2534–41.
[28] Patchornik A, Amit B, Woodward RB. Photosensitive protecting groups. J Am Chem Soc 1970;92:6333–5.
[29] Holmes CP. Model studies for new o-nitrobenzyl photolabile linkers: substituent effects on the rates of photochemical cleavage. J Org Chem 1997;62: 2370–80.
[30] McGall GH, Barone AD, Diggelmann M, Fordor SPA, Gentalen E, Ngo N. The efficiency of light-directed synthesis of DNA arrays on glass substrates. J Am Chem Soc 1997;119:5081–90.
[31] Shin DS, Lee KN, Jang KH, Kim JK, Chung WJ, Kim YK, et al. Protein patterning by maskless photolithography on hydrophilic polymer-grafted surface. Biosens Bioelectron 2003;19:485–94.
[32] Kim JK, Shin DS, Chung WJ, Jang KH, Lee KN, Kim YK, et al. Effects of polymer grafting on a glass surface for protein chip applications. Colloid Surface B 2004;33:67–75.
[33] van Wachem PB, Hogt AH, Beugeling T, Feijen J, Bantjes A, Detmers JP, et al. Adhesion of cultured human endothelial cells onto methacrylate polymers with varying surface wettability and charge. Biomaterials 1987;8:323–8.
[34] Arima Y, Iwata H. Effect of wettability and surface functional group on protein adsorption and cell adhesion using well-defined mixed self-assembled monolayers. Biomaterials 2007;28:3074–82.
[35] Xu Y, Takai M, Konno T, Ishihara K. Microfluidic flow control on charged phospholipid polymer interface. Lab Chip 2007;7:199–206.
[36] Sigal GB, Mrksich M, Whitesides GM. Effect of surface wettability on the adsorption of proteins and detergents. J Am Chem Soc 1998;120:3464–73.
[37] Roach P, Farrar D, Perry CC. Interpretation of protein adsorption: surface-induced conformational changes. J Am Chem Soc 2005;127:8168–73.
[38] Zelzer M, Majani R, Baradley JW, Rose FRAJ, Davies MC, Alexander MR. Investigation of cell-surface interactions using chemical gradients formed from plasma polymers. Biomaterials 2008;29:172–84.
[39] Faucheux N, Schweiss R, Lützow K, Werner C, Groth T. Self-assembled monolayers with different terminating groups as model substrates for cell adhesion studies. Biomaterials 2004;25:2721–30.
[40] Schweikl H, Müller R, Englert C, Hiller KA, Kujat R, Nerlich M, et al. Proliferation of osteoblasts and fibroblasts on model surfaces of varying roughness and surface chemistry. J Mater Sci 2007;18:1895–905.
[41] Lee JH, Lee JW, Khang G, Lee HB. Interaction of cells on chargeable functional group gradient surfaces. Biomaterials 1997;18:351–8.
[42] Kishida A, Iwata H, Tamada Y, Ikada Y. Cell behaviour on polymer surfaces grafted with non-ionic and ionic monomers. Biomaterials 1991;12:786–92.
[43] Fuente JM, Andar A, Gadegaard N, Berry CC, Kingshott P, Riehle MO. Fluorescent aromatic platforms for cell patterning. Langmuir 2006;22:5528–32.
[44] Madri JA, Stenn KS. Aortic endothelial cell migration. Am J Pathol 1982;106:180–6.

Suppression of Protein Adsorption on a Charged Phospholipid Polymer Interface

Yan Xu,*,† Madoka Takai,* and Kazuhiko Ishihara

Department of Materials Engineering, School of Engineering, and Center for NanoBio Integration, The University of Tokyo, 7-3-1, Hongo, Bunkyo-ku, Tokyo 113-8656, Japan

Received September 9, 2008

High capability of a charged interface to suppress adsorption of both anionic and cationic proteins was reported. The interface was covalently constructed on quartz by modifying with an anionic phospholipid copolymer, poly(2-methacryloyloxyethyl phosphorylcholine (MPC)-*co*-*n*-butyl methacrylate (BMA)-*co*-potassium 3-methacryloyloxypropyl sulfonate (PMPS)-*co*-3-methacryloxypropyl trimethoxysilane (MPTMSi)) (PMBSSi). The PMBSSi interfaces were very hydrophilic and homogeneous and could function effectively for a long time even under long-term fluidic working conditions. The PMBSSi density on the interface, which was controllable by adjusting the PMBSSi concentration of the modification solution, affected the surface properties, including the surface contact angle, the surface roughness, and the surface ζ-potential. When a PMBSSi modification was applied, the adsorption of various proteins (isoelectric point varying from 1.0 to 11.0) on quartz was reduced to at least 87% in amount, despite the various electrical natures these proteins have. The protein adsorption behavior on the PMBSSi interface depended more on the PMBSSi density than on the surface charge. The PMBSSi modification had a stable impact on the surface, not only at the physiologic ionic strength, but also over a range of the ionic strength, suggesting that electrostatic interactions do not dominate the behavior of protein adsorption to the PMBSSi surface.

1. Introduction

Prevention of nonspecific protein adsorption is important in various areas, such as biological assays, medical diagnostics, drug discovery, and surgery. Methods to overcome the nonspecific protein adsorption to surfaces have been developed. One way is to physically or chemically modify the surface of the material. Various surface modification materials including polymers have been finely reviewed in literature.[1,2] Among them, one of the most attractive polymers is poly(2-methacryloyloxyethyl phosphorylcholine) (poly(MPC)) and its derivatives.[3,4] The concept behind the incorporation of phosphorylcholine(PC) moieties onto surfaces by modification with MPC polymers evolved from the fact that the zwitterionic phospholipids, which are major components of the cell membrane, have been shown to significantly resist protein adsorption. Accordingly, the MPC polymers possess excellent biological and biomedical benefits from a bulk class to micro- and nanoscales.[5−7] Especially in the novel field of microfluidic chip devices (or the so-called micrototal analysis systems (μ-TAS) and lab-on-a-chip systems), which have promised a new era of chemistry, biology, and medicine in miniaturized systems, recently we have developed several MPC polymers to modify major chip substrate materials.[8,9] For example, poly(MPC-*co*-*n*-butyl methacrylate (BMA)) (PMB), which has shown biocompatibility to human whole blood, was successfully applied to a microcapillary chip for a blood serum assay.[10] To our knowledge, this is the first time the MPC moieties have been immobilized in a microfluidic chip. In addition, poly(MPC-*co*-3-methacryloxypropyl trimethoxysilane (MPTMSi)) (PMSi), a copolymer composed of the MPC and a methacrylate with a silane coupling moiety (MPTMSi), by which we have constructed a MPC polymer covalent coating via a silanization process in a glass microchip.[11] We have demonstrated that the PMSi coating could effectively suppress both protein adsorption and cell adhesion in an electro-osmotic flow (EOF) actuated cell sorter chip. The EOF, as a state-of-the-art approach widely applied in miniaturized systems for fluid delivery, offers many advantages, features such as easy control and simple miniaturization.[12] Nevertheless, the EOF in the PMSi-coated microchannel was too weak to efficiently handle cells, because PMSi is a neutral polymer with a ζ-potential of nearly 0 mV. Other researchers have also successfully developed some neutral polymers to resist nonspecific protein adsorption in microfluidic chips, but they have the same limitation as PMSi in the EOF generation.[13]

To explore the possibility and capability of applying the MPC polymer to electrokinetically actuated microfluidic chips with biological applications, it is very necessary to further modify the polymer architecture of the recently available PMSi with incorporating the charge. Potassium 3-methacryloyloxypropyl sulfonate (PMPS), which contains an anionically charged group, was therefore first introduced for this purpose. While Lewis et al. has reported incorporation of cationic moieties within a MPC copolymer to selectively induce interactions between the coated surface and cells or other molecules,[14] to induce the EOF, anionic moieties are generally considered to be favorable. As a methacrylate monomer, PMPS not only is commercially available and well documented in literature,[15,16] but also has reactivity to the other methacrylate monomers such as MPC.[17] As described above, the structure of the modified PMSi is poly(MPC-*co*-BMA-*co*-PMPS-*co*-MPTMSi) and is referred to as PMBSSi. In a preceding paper, we detailed the synthesis and characterization of PMBSSi and emphasized on the electrokinetic properties of the PMBSSi-coated

* To whom correspondence should be addressed. Tel.: +81-3-5841-7233 (Y.X.); +81-3-5841-7125 (M.T.). Fax: +81-3-5841-6039 (Y.X.); +81-3-5841-8647 (M.T.). E-mail: xuyan@icl.t.u-tokyo.ac.jp (Y.X.); takai@mpc.t.u-tokyo.ac.jp (M.T.).

† Present address: Department of Applied Chemistry, School of Engineering, The University of Tokyo.

10.1021/bm801279y CCC: $40.75
Published on Web 12/18/2008

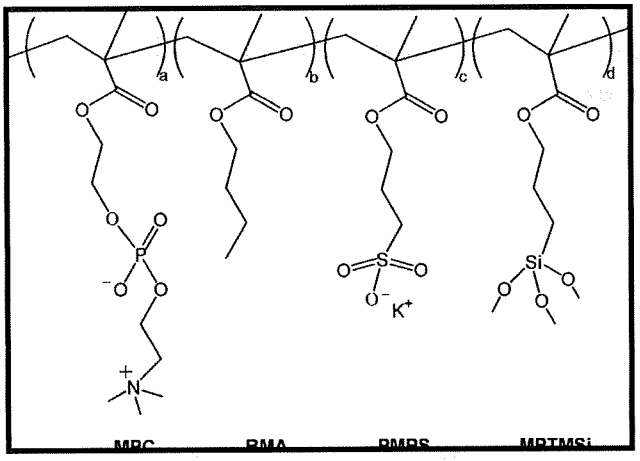

Figure 1. Chemical structure of poly(MPC-*co*-BMA-*co*-PMPS-*co*-MPTMSi) (PMBSSi).

quartz.[18] The surface ζ-potential was seen to increase with the increase of the polymer concentration for coating. Consequently, the magnitude of the EOF in the modified microchannel could be modulated by only adjusting the coating concentration. Because this control is dependent on surface differences rather than the change in the buffer composition of many conventional methods, it would be more suited to miniaturized systems for biological applications requiring neutral buffer conditions. Importantly, the study primarily revealed that the anionically charged groups of PMBSSi had no unfavorable effect on the suppression of protein adsorption. This suggests that the possibly increased electrostatic interactions from the surface charge may not dominate the protein adsorption/desorption process in the PMBSSi system. To elucidate this point, the relationships between various factors and the resistance of protein adsorption should be further investigated. These factors would include surface properties, protein properties, and buffer properties, which are generally thought as key factors involved in the process of the protein adsorption to surfaces.[19,20] Herein we, in particular, describe and discuss how these factors affect the suppression of protein adsorption when the charged MPC polymer coating is applied and thereby try to elucidate the ability of MPC to resist protein adsorption when it consists in a copolymer system with other charged moieties. This not only is certainly important for charged MPC polymers to be applied in microfluidic devices as well as other biomedical fields, but also would be meaningful for elucidating the mechanism of the protein adsorption to a charged surface.

2. Experimental Section

Synthesis of Anionic Phospholipid Copolymer. The anionic phospholipid copolymer, poly(MPC-*co*-BMA-*co*-PMPS-*co*-MPTMSi) (PMBSSi, shown in Figure 1), was synthesized according to the process described by us previously.[18] In summary, first, the desired amounts of MPC (synthesized as reported by us elsewhere),[21] BMA (Kanto Chemicals, Tokyo, Japan), PMPS (Tokyo Kasei Kogyo Co., Tokyo, Japan), MPTMSi (Kanto Chemicals), and α,α′-azobisisobutyronitrile (AIBN, Kanto Chemicals, as initiator) were dissolved in ethanol in a flask at room temperature. Then the radical polymerization was performed in the sealed flask at 60 °C for 6 h. Finally, the polymer product was reprecipitated from an ether/chloroform (7/3, v/v) mixture solvent and dried in vacuo. The structure of the copolymer was identified by ^{1}H NMR. The average molecular weight (M_w) was determined by a gel permeation chromatography (GPC) system (JASCO International Co., Ltd., Tokyo, Japan). The molecular properties of PMBSSi are listed in Table 1.

Surface Coating. Quartz substrates (Sendai Quartz and Glass, Sendai, Japan) with 0.5 mm thickness were used for coating. The PMBSSi ethanol solutions were used as coating solutions without any additives. After being cleaned by ethanol and O_2 plasma treatment, the substrate was ready for a dip-coating procedure: the cleaned substrate was first immersed in the polymer solution of the desired concentration for 2 h, then, the substrate was dried under nitrogen, and after that, the coated substrate was further dried in a vacuum condition overnight. Before being used for characterization and investigation, the samples were first rinsed by the distilled water to wash off the remained unreacted PMBSSi molecules, then dried under nitrogen, and dried again in a vacuum condition overnight.

Surface Characterization. *XPS Analysis.* The surface elemental composition was determined by X-ray photoelectron spectroscopy (XPS) (Axis-His, Shimadzu/KRATOS, Kyoto, Japan). XPS analyses were carried out under a high vacuum condition of 1×10^{-9} Torr or less. The X-ray source was Mg Kα (1253.6 eV) and the electric current was 10 mA. The takeoff angle employed was 90°. For each sample, three samples were analyzed.

Evaluation of Coating Stability. The quartz plates coated with PMBSSi were first fixed with stainless wires and then rinsed in distilled water undergoing magnetic stirring at 300 rpm. All the plates were kept under the same rinsing conditions. The plates were removed after rinsing for 1, 5, 25, and 45 h. The elemental compositions on the surfaces of the rinsed plates were analyzed by XPS. At least three samples for each rinsing duration were measured. As controls, samples without fluidic rinsing were also measured (i.e., elemental compositions at 0 h).

Coating Density Measurement. The coating density was determined with a quartz crystal microbalance (QCM). QCM has been widely used to measure the mass of material/molecules attached to the surface of the quartz crystal via changes in the resonant frequency (Δf).[22,23] The resonant frequency of the sensor crystal (f) depends on the total oscillating mass. When a thin film is attached to the sensor crystal, the frequency decreases. The resonant frequency shift of the QCM is due to the change in the total coupled mass. If the film is thin and rigid, the decrease in frequency is proportional to the mass of the film. In this way, the QCM operates as a very sensitive balance. The mass of the adhering layer is calculated by using the Sauerbrey relation[24]

$$\Delta m = -\frac{C \cdot \Delta f}{n} \quad (1)$$

where C (= 17.7 ng Hz^{-1} cm^{-2} for f = 5 MHz crystals) is the mass sensitivity constant and n (= 1, 3,...) is the overtone number. In this study, all measurements were performed using a Q-Sense D300 system (Q-Sense AB, Göteborg, Sweden). The Q-Sense software package was employed to acquire experimental data and to evaluate the data with modeling fittings. For the accurate modeling, the measuring at multiple frequencies (i.e., 5, 15, 25, and 35 MHz) was simultaneously applied. The SiO_2 coated (SiO_2/Au) sensor crystal was first cleaned by reactive oxygen plasma. Then the resonant frequency of the sensor crystal (f_c) was previously measured. Next, the active side of the sensor crystal was spin-coated with the PMBSSi solution of the desired concentration. After that, the PMBSSi coated sensor was dried in a vacuum condition overnight. To wash off the remaining unreacted PMBSSi, the coated crystal was rinsed with distilled water, dried under nitrogen, and further dried in a vacuum condition overnight. Finally, the resonant frequency of the PMBSSi coated sensor crystal (f_p) was measured. In this case, ($f_p - f_c$) is the change in the resonant frequency (Δf), by which the mass of PMBSSi per unit area (defined as *coating density*) can be calculated through the Sauerbrey relation. Because the coating process for a sensor crystal is almost the same as that for a quartz substrate, the PMBSSi coating on the sensor is considered identical with that on the quartz substrate.

Contact Angle Measurement. The static water contact angle of the surface was measured by using a CA-W automatic contact angle meter (Kyowa Interface Science, Saitama, Japan); for each sample, at least six different areas were measured and averaged.

AFM Analysis. The surface morphology was characterized by an atomic force microscopy (AFM; Bioscope, Nanoscope IIIa, Veeco,

Table 1. Molecular Properties of PMBSSi

abb.	composition (mole fraction)[a] [MPC/BMA/PMPS/MPTMSi]	molecular weight (M_w)[b]	polydispersity ratio (M_w/M_n)[c]	solubility[d] H_2O	solubility[d] EtOH
PMBSSi	46/32/9/13	1.2×10^4	1.2	+	+

[a] Determined by ^{1}H NMR. [b] Weight average molecular weight (M_w); determined by GPC, PEO standard. [c] M_n: number average molecular weight. [d] Evaluated by dissolving 0.1 g polymer powder in a 10 mL solvent; +: soluble.

Table 2. Properties and Related Information of Proteins Used in the Study

proteins[a]	approximate isoelectirc point (*pI*)	approximate molecular weight (M_w)/kDa	source
pepsin	1.0	35.0	porcine stomach mucosa
albumin	4.7	66.0	bovine serum
fibrinogen	5.5	340.0	bovine plasma
γ-globulins	5.8–7.3	150.0	bovine blood
hemoglobin	6.8–7.0	64.5	bovine blood
myoglobin	7.0/7.4	17.6	horse skeletal muscle
α-chymotrypsin	8.8	25.0	bovine pancreas
ribonuclease A	9.5	13.7	bovine pancreas
cytochrome c	10.0–10.5	12.4	horse heart
lysozyme	11.0	14.3	chicken egg white

[a] Except for myoglobin (Wako Pure Chemical Industries, Ltd., Tokyo, Japan), all the other proteins were purchased from Aldrich-Sigma (St. Louis, MO).

Santa Barbara, CA). Measurements under dry conditions were performed using the tapping mode of operation with a phosphorus (n) doped silicon cantilever (RTESP). For in situ AFM measurements in solution (1X Dulbecco's Phosphate-Buffered Saline (D-PBS), pH 7.1, Invitrogen Company, Carlsbad, CA) wet condition, a nonconductive silicon nitride cantilever (NP-S20) was used in tapping mode in the fluid. The roughness of the surface topographies (10×10 μm^2 area) was characterized by measuring the root-mean-square (rms) roughness of the AFM images.

Surface ζ-Potential Measurement. The surface ζ-potential was measured in a 10 mM NaCl solution using an electrophoretic light-scattering spectrophotometer (ELS 8000, Otsuka Electron., Osaka, Japan) with a plate cell; for every sample, the determination was repeated six times.

EOF Measurement. A method taking advantage of the migration data collected with a suitable neutral and inert tracer in an open channel under an applied electric field was applied to estimate the EOF mobility. This method has been presented elsewhere,[25] including in our previous work.[18] In this research, the measurements of the EOF behaviors were performed using the microchannel with polystyrene microspheres (Polybead) as neutral tracers, whose average diameter was 6.0 μm. 1X D-PBS (adjusted to pH 7.0) was used as a buffer in the measurements.

Investigation of Protein Adsorption. The evaluation of the protein adsorption was conducted on the quartz substrates ($20 \times 20 \times 0.5$ mm^3) with various proteins listed in Table 2. Protein solutions (0.32 g L^{-1}) prepared in 1X D-PBS buffer (pH 7.1) were used for all the experiments except for studies on ionic strength effect on the amount of adsorption, in which additional NaCl (50 and 150 mM) was spiked in the 1X D-PBS to given concentrations. The protocol for determining the amount of protein adsorption on a sample surface is described as follows. First, after the coated and uncoated (control) quartz plates were equilibrated overnight in distilled water, they were immersed in 10 mL of protein solution and incubated at 37 °C for 1 h to achieve adequate contact between the quartz plates and the protein. Then the plates were removed and rinsed in sufficient 1X D-PBS (pH 7.1), undergoing 300 rpm magnetic stirring to remove the unabsorbed protein; this rinsing procedure was conducted twice for 5 min each time. To detach all the adsorbed protein from the quartz plate, each plate was placed in a small case with 2.0 mL of 10 mg mL^{-1} sodium dodecyl sulfate (SDS) solution (water as solvent) in which the quartz plate was adequately immersed. The sealed case was treated via ultrasonication for 10 min, and the amount of protein in the SDS solution was determined by the Micro BCA protocol (Micro BCA Protein Assay Kit, Pierce Biotechnology, Rockford, IL).[26]

3. Results and Discussion

Preparation of Charged Phospholipid Copolymer Coating. Table 1 shows the molecular properties of PMBSSi. The MPTMSi moieties in the synthesized anionic phospholipid copolymer (PMBSSi) possess silanization reactivity. A silanization process is an effective way to chemically change the surface properties of silica-based substrates, because these substrates contain hydroxyl groups which attack and displace the alkoxy groups on the silane-coupling agents thus forming a covalent -Si−O−Si- bond. The silanization strategy has been widely applied in microfluidic chip devices for surface modification, because silica-based substrates such as quartz and glass are initial and popular substrate materials to fabricate and develop microfluidic devices. British workers have first reported an incorporation of silane-coupling moieties in a MPC copolymer for inducing cross-linking among polymer molecules,[27] while we have first constructed a MPC polymer interface via a silanization process in a quartz microchip by a MPC polymer composed of MPC and MPTMSi.[11] In this study, the MPTMSi moieties were also incorporated for the same purpose. After hydrolysis, the PMBSSi macromolecules attack the hydroxyl groups of the SiO_2 substrate, thus forming a covalent -Si−O−Si- bond via a dehydration process (with heat or in vacuo). In the synthesized PMBSSi, the mole fraction of the MPTMSi moieties is 13%. This composition is sufficient because, as reported in our previous research, a composition of 10% (mole fraction) MPTMSi in copolymer was sufficient to make a covalent coating on quartz.[11] In PMBSSi, the mole fraction of MPC units is 46%. This is a composition in consideration of both the suppression of the protein adsorption and the solubility of the copolymer because the MPC copolymer having more than 30% MPC units in mole fraction is apt to dissolve in water and some other representative protic solvents such as ethanol.[28] In fact, PMBSSi can be dissolved in both water and ethanol, which is favorable in surface modifications of various devices, especially microfluidic devices. Therefore, alcoholic solutions of PMBSSi were used as coating solutions without any other additives. This enables easy handling, quick treatment, and nearly no solvent remnants after treatment. The coating process is very simple, as described in Experimental Section, just a conventional dip coating, and can be quickly completed in 2 h.

XPS analysis was used to confirm the modification of the quartz surface. The binding energy (BE) scale was corrected using C_{1s} as a reference at BE = 285 eV. The six elements present in PMBSSi can be identified from their XPS peaks: silicon (Si_{2p}, BE ~ 102 eV), phosphorus (P_{2p}, BE ~ 133 eV), sulfur (S_{2p}, BE ~ 168 eV), carbon (C_{1s}, BE ~ 285 eV), nitrogen (N_{1s}, BE ~ 402 eV), and oxygen (O_{1s}, BE ~ 533 eV). The spectra of nitrogen (N_{1s}) and phosphorus (P_{2p}) at a takeoff angle of 90° were shown in Figure 2. Nitrogen (N_{1s}) and phosphorus (P_{2p}) were detected on both the high-concentration (3.00 mg mL^{-1}) and low-concentration (0.30 mg mL^{-1}) PMBSSi coated

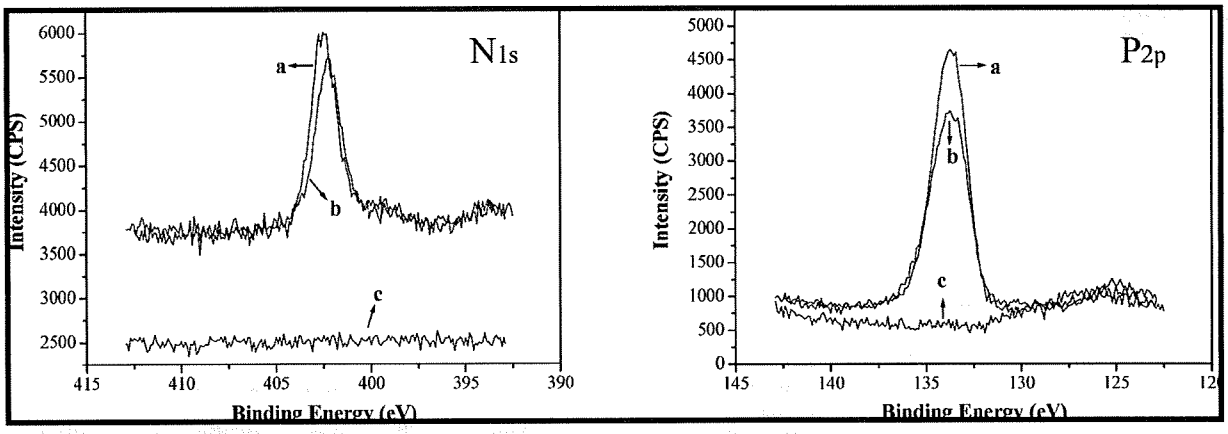

Figure 2. XPS spectra of nitrogen (N_{1s}) and phosphorus (P_{2p}) on different sample surfaces: (a) quartz surface with a high-concentration (3.00 mg mL^{-1}) PMBSSi coating (i.e., high-density coating sample); (b) quartz surface with a low-concentration (0.30 mg mL^{-1}) PMBSSi coating (i.e., low-density coating sample); (c) uncoated quartz surface (i.e., noncoating sample). The spectra were recorded using a takeoff angle of 90° with respect to the sample surface.

surfaces but not on the uncoated quartz surface, indicating the presence of MPC units on the coated surfaces and therefore the success of the surface modification. In addition, the relative peak intensities of both elements were decreased with increasing the concentration of PMBSSi, implying that comparing with the high-concentration coating, the low-concentration coating might make more amount of PMBSSi reacted on the substrate.

Surface Properties. As XPS analyses suggest, the concentration of the polymer coating solution may influence the amount of polymer coated to the quartz surface. To confirm this, we further determined the densities of coatings by a method with the QCM. The modeling with the Q-sense software program indicated that in the case of the high-concentration (3.00 mg mL^{-1}) PMBSSi coating, the resulting thickness of the coating is 87 nm, while the Sauerbrey relation resulted in 88 nm, meaning that this particular film could just be analyzed by the Sauerbrey relation. The coating surface densities of the high-concentration (3.00 mg mL^{-1}) and low-concentration (0.30 mg mL^{-1}) PMBSSi coated surfaces measured by the QCM were 11.14 ± 0.05 $\mu g\ cm^{-2}$ and 1.19 ± 0.01 $\mu g\ cm^{-2}$, respectively. This indicates that the coating density of the high-concentration (3.00 mg mL^{-1}) PMBSSi coating is almost 10 times higher than that of the low-concentration (0.30 mg mL^{-1}) PMBSSi coating, a same difference as exhibited in coating concentrations. Figure 3 demonstrates the relationship between the polymer coating concentration and the coating density. In the figure, noncoating (density = 0.00 $\mu g\ cm^{-2}$), low-density coating (density = 1.19 $\mu g\ cm^{-2}$), and high-density coating (density = 11.14 $\mu g\ cm^{-2}$) represent the uncoated, low-concentration (0.30 mg mL^{-1}) PMBSSi coated and high-concentration (3.00 mg mL^{-1}) PMBSSi coated quartz surfaces, respectively. A linear fit is applicable to describe the relationship between the coating concentration and the coating density, which reveals that the coating density can be adjusted by changing the coating concentration of the polymer solution.

The coating density affected the surface properties including the surface contact angle, the surface roughness and the surface ζ-potential. These surface properties of different samples are listed in Table 3. After the quartz surfaces were coated with PMBSSi, the water contact angle on the surface decreased from 31.2 ± 1.2 degree (noncoating) to 23.8 ± 2.8 degree in the case of the low-density coating and to 13.4 ± 1.3 degree in the case of the high-density coating. The uncoated quartz surface is hydrophilic and the decrease in the contact angle after coating indicates that the coating made the surface more hydrophilic

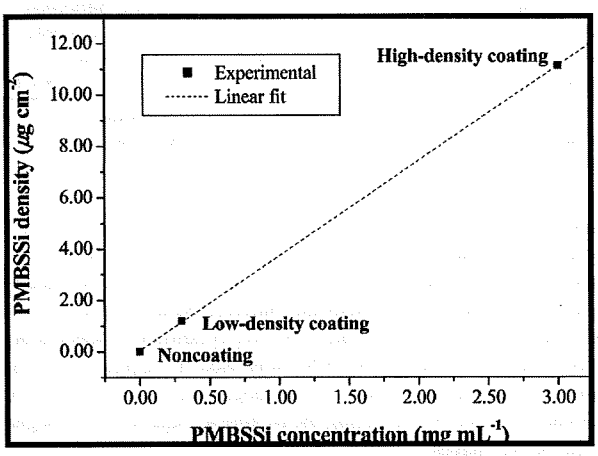

Figure 3. PMBSSi densities on sample surfaces plotted vs PMBSSi concentrations for coating. A linear fit ($y = 0.04 + 3.70x$, $R^2 = 1.00$) is applicable to describe the relationship between the PMBSSi coating density and the PMBSSi concentration for coating.

than the original surface. The rms roughness analyses of AFM observations can provide quantitative information on surface homogeneity. On the one hand, all the samples (noncoating, low-density coating, and high-density coating) exhibited quite low rms roughness values less than 0.80 nm under both dry and PBS wet conditions, indicating that these sample surfaces were homogeneous under both conditions. On the other hand, the calculated rms values also exhibited some subtle changes in roughness as a result of the coating. For example, the rms roughness in dry condition decreased from 0.51 (noncoating) to 0.30 nm (low-density coating) and 0.32 nm (high-density coating) after coating. This decrease could be attributed to the filling of the topographical structure with PMBSSi, leading to smoother surfaces. In addition, the high-density coating had almost the same rms value (0.32 nm) as that of the low-density coating (0.30 nm) in dry conditions. Under PBS wet conditions, the PMBSSi coatings changed the topologies of the surfaces, increasing the roughness values, yielding rms values of 0.79 and 0.69 nm for the low-density coating and the high-density coating, respectively. This increase would be due to the stretching and swelling of the PMBSSi chains in PBS. Surface charge conditions were characterized with the surface ζ-potential. As determined, the quartz surface is negatively charged with a ζ-potential of −47.4 ± 0.9 mV. After coating with PMBSSi, the surface ζ-potential changed, because charged moieties (PMPS moieties) on PMBSSi in place of hydroxyl

Table 3. Surface Properties of Different Sample Surfaces

sample	density[a] (μg cm^{-2})	contact angle[b] (°)	rms roughness (nm) dry	rms roughness (nm) wet	ζ-potential[c] (mV)
noncoating	0.00	31.2 ± 1.2	0.51	0.60	−47.4 ± 0.9
low-density coating	1.19 ± 0.01	23.8 ± 2.8	0.30	0.79	−14.3 ± 1.9
high-density coating	11.14 ± 0.05	13.4 ± 1.3	0.32	0.69	−24.2 ± 2.5

[a] Data are mean ± SD, $n = 3$. [b] Data are mean ± SD, $n \geq 6$. [c] Data are mean ± SD, $n = 6$.

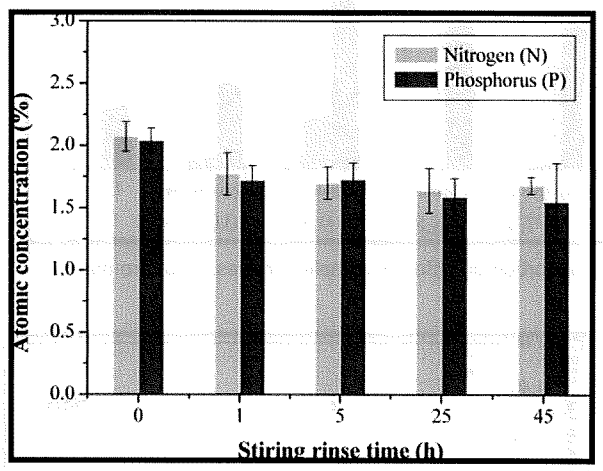

Figure 4. Change in atomic concentration of nitrogen and phosphorus (determined by XPS) on the quartz surfaces with the high-density PMBSSi coatings before (0 h) and after rinsing by stirring at 300 rpm in distilled water for 45 h. Data are mean ± SD, $n = 3$.

groups on the original quartz surface became to dominate the charge condition of the outmost surface. Table 3 indicates that, the low-density coating exhibited a lower (absolute value of) surface ζ-potential (−14.3 ± 1.9 mV) than the high-density coating (−24.2 ± 2.5 mV), owing to the lower amount of PMPS moieties on the low-density coating than on the high-density coating. The coating density further influenced the electrokinetic property of the surface by altering the surface ζ-potential. The EOF determination indicated that the PMBSSi-coated quartz surface retained a significant amount of cathodic EOF.[18] For example, in the condition of 1X D-PBS (adjusted to pH 7.0), the EOF mobility of a quartz microchannel with the high-density PMBSSi coating was (0.99 ± 0.14) × 10^{-4} cm^2 V^{-1} s^{-1}, which is roughly more than half (53%) that of the uncoated microchannel under the same buffer conditions.

The evaluation of the coating stability provided evidence that the PMBSSi coating is a type of stable coating. The investigations were carried out in distilled water undergoing a quite high speed of magnetic stirring (300-rpm). As demonstrated in Figure 4, the surface atomic concentrations of nitrogen (N) and phosphorus (P) on the quartz surfaces with high-density PMBSSi coatings, which were determined by XPS, remained at almost the same levels during the entire long-term (45 h) rinse process. Therefore, the PMBSSi coating layer could not be detached by the fluidic rinse. This reveals that the PMBSSi coating can function effectively for a long time even under long-term fluidic working conditions.

Suppressing Protein Adsorption by Coating. To investigate the ability of the charged polymer coating to suppress protein adsorption, various proteins with different isoelectric points (*pI*), a critical pH point at which a protein carries no net electrical charge, were employed to quantitatively evaluate protein adsorptions on coated quartz surfaces. The information of these proteins is listed in Table 2. All the samples were analyzed by the MicroBCA protein analysis protocol, which is usually applied to determine protein amounts in solutions with very low protein concentrations.[26] In the same batch, uncoated quartz surfaces were also analyzed as controls. All the protein solutions were prepared in 1X D-PBS (pH 7.1), which is a physiological buffer condition that is conventionally applied in many biological analyses. The results are arranged based on the *pI* values of the proteins in order to elucidate the effects of the charge conditions of the PMBSSi coatings on protein adsorption. The results are shown in Figure 5. All proteins, both the anionic and cationic ones, had high adsorption amounts on the uncoated quartz surfaces, and in contrast, had significantly low adsorption amounts on the PMBSSi coated surfaces. For example, bovine serum albumin (BSA, $pI = 4.7$, anionic) and lysozyme (LYZ, $pI = 11.0$, cationic) had adsorption amounts of 1.47 μg cm^{-2} and 0.35 μg cm^{-2}, respectively, on the uncoated surfaces (noncoating); but these amounts are reduced to 0.17 μg cm^{-2} and 0.02 μg cm^{-2}, respectively, on the surfaces with high-density PMBSSi coatings. When a high-density coating was applied, the amount reduction in adsorption was at least 87% and, in some cases (for example, α-chymotrypsin), was more than 99%. That is to say, proteins, both anionic and cationic ones, hardly adsorb onto the surfaces constructed by PMBSSi, although it is charged.

Effect of Coating Density. The protein adsorption to a surface depends on the surface properties to some extent. As described previously, the differences in surface properties of PMBSSi coating can be essentially attributed to the difference in surface coating density. Hence, it is useful to obtain a relationship between the coating density and the amount of protein adsorbed on the charged surface. Comparing the data of the amounts of adsorbed protein (Figure 5), we found that after coating with PMBSSi, both the high-density coating and the low-density coating caused a dramatic decrease in the protein adsorption. There was, however, some slight difference in the amounts of protein adsorption between the two cases. All the protein adsorption data indicated that the surface with the high-density coating exhibited much lower amounts of protein adsorption than the surface with the low-density coating. For example, taking pepsin ($pI = 1.0$, anionic) and ribonuclease A ($pI = 9.5$, cationic) as instances, in the case of pepsin, the amounts adsorbed on the low- and high-density coatings were 0.55 μg cm^{-2} and 0.18 μg cm^{-2}, respectively, and in the case of ribonuclease A, they were 0.29 μg cm^{-2} and 0.08 μg cm^{-2}, respectively. That is, the amounts of adsorbed protein in both cases deceased with increasing the PMBSSi coating density. The same tendencies in the effect of the coating density were obtained in all the cases of the other proteins. As aforementioned (Table 3), an increase in the PMBSSi density resulted in an increase in the absolute value of the surface ζ-potential. In some conventional surfaces, as the absolute value of the surface ζ-potential increases, the electrostatic interactions between the surface and the protein would increase, and therefore the risk of protein adsorption would also increase.[20] However, in the PMBSSi coated surfaces, the increase in the surface ζ-potential resulted from the increase in the PMBSSi density, did not lead to more amounts of protein adsorbed to the surfaces, and

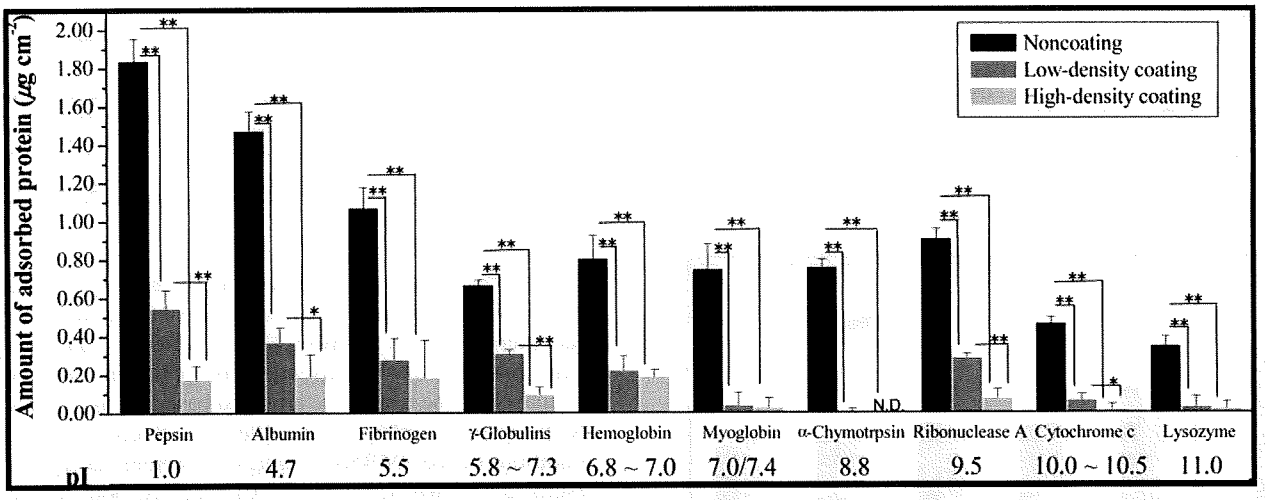

Figure 5. Amounts of various proteins with *pI* values varying from 1.0 to 11.0 absorbed on different sample surfaces. Data are mean ± SD, $n = 9$. Statistical difference significance: *, $p < 0.01$; **, $p < 0.001$.

contrarily, made more reduction in the amount of protein adsorption. This suggests that the PMBSSi density should be the key factor which affects the protein adsorption/resistance on the PMBSSi coated surface. It is known that the PC groups of MPC units play a key role in the suppression of protein adsorption in the MPC polymer coating. More PC groups mean a higher capability to suppress the protein adsorption to some extent. Comparing with the low-density coating, the high-density coating made more PMBSSi react with the quartz surface and thereby afforded a higher composition of MPC units (or PC groups) in the coating layer. This contributed to more reduction in protein adsorption in the high-density coating. In addition, comparing with the high-density coating, the low-density coating has a looser steric structure of coating layer, which may create more chances for some proteins to penetrate into the inner layer of the coating and, consequently, lead to an increase in the amount of protein adsorption. Therefore, in the PMBSSi coating system, we consider that the amount of proteins in the PMBSSi surface might depend more on the PMBSSi density than on the surface charge of the coating.

Effect of Buffer Ionic Strength. The ionic strength of a buffer is generally considered to remarkably affect a protein adsorbing from buffer to a charged surface because counterion concentration affects the degree to which the surface charge is shielded. To further elucidate the role of surface charge in the protein adsorption to PMBSSi coated surfaces, the adsorption behaviors were studied in buffers with different ionic strengths. The increase of the ionic strength was obtained by addition of NaCl to 1X D-PBS. Both BSA and LYZ adsorptions were studied as functions of the addition of NaCl. As shown in Figures 6 and 7, the amounts of BSA and LYZ adsorbed on the uncoated quartz surfaces (noncoating) decreased dramatically with the addition of NaCl in the range of 0 mM to 150 mM. This can be explained by the screened electrostatic interactions occurring at high ionic strength. This reveals that the uncoated quartz surface was intensely sensitive to the electrostatic conditions. However, in contrast to the adsorption behavior on the uncoated quartz surface, which displayed strong ionic strength sensitivity, the BSA adsorption on both the low- and the high-density coated quartz surfaces were not significantly affected by the increase in the ionic strength (Figure 6). The similar behavior also exhibited in the LYZ adsorption, which is shown in Figure 7. These profiles indicate that the PMBSSi coating has an impact on the surface, not only at the physiologic ionic strength but also over a range of the ionic strength.

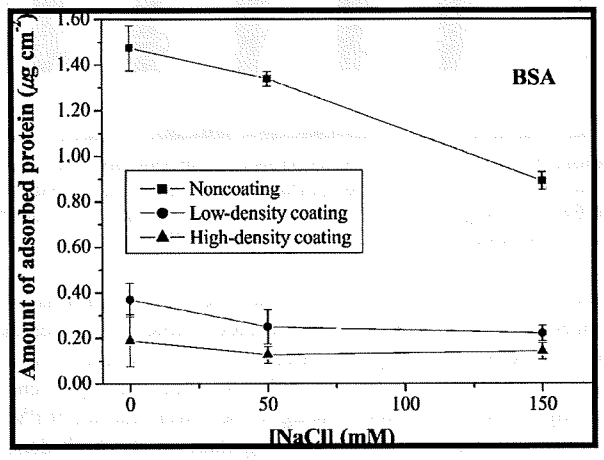

Figure 6. Influence of the buffer ionic strength on the amount of bovine serum albumin (BSA, $pI = 4.7$, anionic) adsorbed on different sample surfaces. The increase of the buffer ionic strength was obtained by addition of NaCl to 1X D-PBS (pH 7.1). [NaCl] represents the added NaCl concentration and the NaCl concentration of original 1X D-PBS (about 137 mM) is not included. Data are mean ± SD, $n = 9$.

Moreover, the buffer ionic strength has no pronounced influence on protein adsorption to the PMBSSi modified surface, suggesting that this process was not dominated by electrostatic interactions between protein molecules and the surface.

Although the understanding of the mechanism and the physics of protein resistance specific to MPC-based surface remains in complete in the present time, several hypotheses or theories have been proposed based on common understandings and our group's research.[4,29,30] The research let us be aware of the importance of exploring water interactions among the surface and around the environment to understand the protein resistance. If the water state at the surface is similar to an aqueous solution, protein does not need to release bound water molecules even if protein molecules contact the surface. This means that the hydrophobic interaction does not occur between proteins and the polymer surface. Moreover, the conformational change in the protein's three-dimensional structure during protein adsorption on or contact with the surface does not happen. Our research elucidated that MPC-based polymers usually carry higher level of free water fraction on the polymer surface, as is well-known that PC groups are highly hydrated. Thus, proteins can contact the surface reversibly, without significant conformational change.

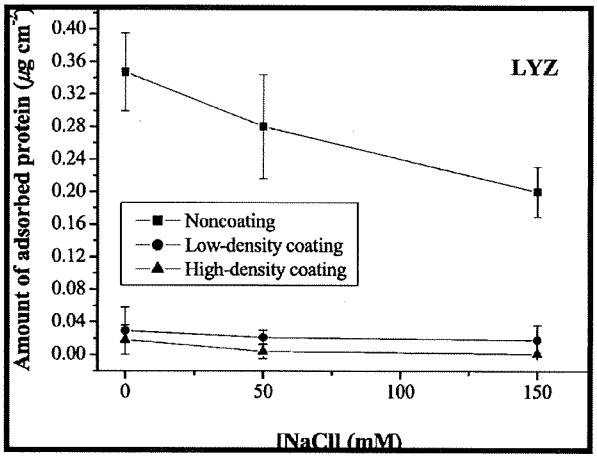

Figure 7. Influence of the buffer ionic strength on the amount of lysozyme (LYZ, *pI* = 11.0, cationic) adsorbed on different sample surfaces. The increase of the buffer ionic strength was obtained by addition of NaCl to 1X D-PBS (pH 7.1). [NaCl] represents the added NaCl concentration and NaCl concentration of original 1X D-PBS (about 137 mM) is not included. Data are mean ± SD, $n = 9$.

The results of the simulation work suggested that PC head groups are very quickly surrounded and polarized by the water molecules when contacting with water.[31] Further, Kitano et al. found that the structure of the aqueous solution surrounded PC groups is very close to that of pure water by the Raman spectrum.[32]

As charged units (PMPS) involved, however, PMBSSi is more complicated than other noncharged MPC polymers. In this work, the experimental results suggest that the amount of surface charge was shown to be a poor determinant of protein adsorption (Figure 5). Accordingly, the effect of electrostatic interactions on the adsorption of the proteins studied is minimal or neglectable (Figures 6 and 7). This tests and supports the hypothesis proposed by Lewis, A. L. that, even though the surface charge of the MPC polymer coating is changed by incorporation of the monomer having charged groups, if a significant proportion of PC in the composition exists, the interaction of the protein with the charged surface may still be similar to that with a surface of a noncharged MPC polymer coating.[33] This group demonstrated adding cationic charge to MPC polymer with the cationically charged monomer choline methacrylate (CMA), that all polymer coatings containing 0−23% CMA (mole fraction, converted from the weight percentage originally described by the authors in the reference) exhibited small amounts of protein adsorption, with no statistical difference.[33] In the PMBSSi, the mole fraction of MPC monomers is 46%, which is predominant among all components. In contrast, the anionically charged monomer PMPS is only 9% in mole fraction, an amount that is considered incapable of inducing significant amounts of protein adsorption. In addition, in the case of the PMBSSi coating, the increase of the buffer ionic strength by addition of NaCl does not remarkably change the property of the PC dominated interface, so it does not significantly affect the resistance of protein adsorption on the surface. Therefore, the charge in the PMBSSi not only satisfies the requirement for generation of the electrokinetic phenomena but also has no adverse effect on suppression of the protein adsorption.

4. Conclusions

We described a charged interface constructed on the silica-based substrate with a charged phospholipid copolymer (PMBSSi) coating with the covalent bonding, which has high capability to suppress adsorption of both anionic and cationic proteins. The PMBSSi interfaces were very hydrophilic and homogeneous, and could function effectively for a long time even under long-term fluidic working conditions. The coating density, which was controllable by adjusting the polymer coating concentration, affected the surface properties including the surface contact angle, the surface roughness and the surface ζ-potential. When a PMBSSi coating was applied, the adsorption of various proteins with a wide range of *pI* (1.0−11.0) on quartz was suppressed significantly to at least 87% in amount. The high-density coating, though exhibited a higher surface ζ-potential, showed much higher reduction in the amount of protein adsorption in comparison with the low-density coating, indicating that the protein adsorption behavior on the PMBSSi interface depends more on the surface density than on the surface charge. This was explained by the fact that the higher density coating affords more composition of PC groups on the interface when on contact with water. Further, in contrast to the adsorption behavior on the uncoated quartz surface, which displayed strong ionic strength sensitivity, protein adsorption on PMBSSi coated quartz surfaces were not remarkably affected by the change in the ionic strength. That is, the PMBSSi coating has an impact on the surface, not only at the physiologic ionic strength but also over a range of the ionic strength, revealing that electrostatic interactions do not dominate the behavior of protein adsorption to the PMBSSi surface. Therefore, the PMBSSi interface holds the capability to be applied to electrokinetically actuated microfluidic chips with biological applications, for not only suppressing the unfavorable protein adsorption but also simultaneously generating favorable electrokinetic phenomena.

Acknowledgment. This study was supported in part by Scientific Research(B) 16310084 from Grants-in-Aid for Scientific Research of Japan Society for the Promotion of Science (JSPS) and by Asahi Glass Foundation (2004).

References and Notes

(1) Werner, C.; Maitz, M. F.; Sperling, C. *J. Mater. Chem.* **2007**, *17*, 3376–3384.
(2) Jordan, S. W.; Chaikof, E. L. *J. Vasc. Surg.* **2007**, *45*, 104A–115A.
(3) Iwasaki, Y.; Ishihara, K. *Anal. Bioanal. Chem.* **2005**, *381*, 534–546.
(4) Ishihara, K.; Nomura, H.; Mihara, T.; Kurita, K.; Iwasaki, Y.; Nakabayashi, N. *J. Biomed. Mater. Res.* **1998**, *39*, 323–330.
(5) Feng, W.; Zhu, S. P.; Ishihara, K.; Brash, J. L. *Biointerphases* **2006**, *1*, 50–60.
(6) Kaji, H.; Kawashima, T.; Nishizawa, M. *Langmuir* **2006**, *22*, 10784–10787.
(7) Goto, Y.; Matsuno, R.; Konno, T.; Takai, M.; Ishihara, K. *Biomacromolecules* **2008**, *9*, 828–833.
(8) Sakai-Kato, K.; Kato, M.; Ishihara, K.; Toyo'oka, T. *Lab Chip* **2004**, *4*, 4–6.
(9) Sibarani, J.; Takai, M.; Ishihara, K. *Colloid Surf., B* **2007**, *54*, 88–93.
(10) Oki, A.; Adachi, S.; Takamura, Y.; Ishihara, K.; Ogawa, H.; Ito, Y.; Ichiki, T.; Horiike, Y. *Electrophoresis* **2001**, *22*, 341–347.
(11) Takai, M.; Onoda, H.; Ishihara, K.; Takamura, Y.; Horiike, Y. In *Micro Total Analysis Systems 2004*, Laurell, T., Nilsson, J., Jensen, K., Harrison, D. J., Eds.; Royal Soc. Chem.: Cambridge, U.K., 2005; Vol. 2, pp 115−117.
(12) Stone, H. A.; Stroock, A. D.; Ajdari, A. *Annu. Rev. Fluid Mech.* **2004**, *36*, 381–411.
(13) Wu, D. P.; Zhao, B. X.; Dai, Z. P.; Qin, J. H.; Lin, B. C. *Lab Chip* **2006**, *6*, 942–947.
(14) Lewis, A. L.; Berwick, J.; Davies, M. C.; Roberts, C. J.; Wang, J. H.; Small, S.; Dunn, A.; O'Byrne, V.; Redman, R. P.; Jones, S. A. *Biomaterials* **2004**, *25*, 3099–3108.
(15) Masci, G.; Bontempo, D.; Tiso, N.; Diociaiuti, M.; Mannina, L.; Capitani, D.; Crescenzi, V. *Macromolecules* **2004**, *37*, 4464–4473.
(16) Roland-Swanson, C.; Besse, J. P.; Leroux, F. *Chem. Mater.* **2004**, *16*, 5512–5517.

(17) Ito, T.; Iwasaki, Y.; Narita, T.; Akiyoshi, K.; Ishihara, K. *Colloid Surf., B* **2005**, *41*, 175–180.
(18) Xu, Y.; Takai, M.; Konno, T.; Ishihara, K. *Lab Chip* **2007**, *7*, 199–206.
(19) Glomm, W. R.; Halskau, O.; Hanneseth, A. M. D.; Volden, S. *J. Phys. Chem. B* **2007**, *111*, 14329–14345.
(20) Pasche, S.; Voros, J.; Griesser, H. J.; Spencer, N. D.; Textor, M. *J. Phys. Chem. B* **2005**, *109*, 17545–17552.
(21) Ishihara, K.; Ueda, T.; Nakabayashi, N. *Polym. J.* **1990**, *22*, 355–360.
(22) Marx, K. A. *Biomacromolecules* **2003**, *4*, 1099–1120.
(23) Andersson, M.; Andersson, J.; Sellborn, A.; Berglin, M.; Nilsson, B.; Elwing, H. *Biosens. Bioelectron.* **2005**, *21*, 79–86.
(24) Sauerbray, G. Z. *Phys.* **1959**, *155*, 206–222.
(25) Rathore, A. S. *Electrophoresis* **2002**, *23*, 3827–3846.
(26) Pierce Biotechnology, Inc. Pierce 2003−2004 Applications Handbook and Catalog; Pierce Biotechnology, Inc.: Rockford, IL, 2003, pp 241−243.
(27) Lewis, A. L.; Cumming, Z. L.; Goreish, H. H.; Kirkwood, L. C.; Tolhurst, L. A.; Stratford, P. W. *Biomaterials* **2001**, *22*, 99–111.
(28) Konno, T.; Watanabe, J.; Ishihara, K. *J. Biomed. Mater. Res., Part A* **2003**, *65*, 209–214.
(29) Ishihara, K.; Oshida, H.; Endo, Y.; Ueda, T.; Watanabe, A.; Nakabayashi, N. *J. Biomed. Mater. Res.* **1992**, *26*, 1543–1552.
(30) Morisaku, T.; Watanabe, J.; Konno, T.; Takai, M.; Ishihara, K. *Polymer* **2008**, *49*, 4652–4657.
(31) Sheng, Q.; Schulten, K.; Pidgeon, C. *J. Phys. Chem.* **1995**, *99*, 11018–11027.
(32) Kitano, H.; Imai, M.; Mori, T.; Gemmei-Ide, M.; Yokoyama, Y.; Ishihara, K. *Langmuir* **2003**, *19*, 10260–10266.
(33) Palmer, R. R.; Lewis, A. L.; Kirkwood, L. C.; Rose, S. F.; Lloyd, A. W.; Vick, T. A.; Stratford, P. W. *Biomaterials* **2004**, *25*, 4785–4796.

BM801279Y

RAFT Synthesis and Stimulus-Induced Self-Assembly in Water of Copolymers Based on the Biocompatible Monomer 2-(Methacryloyloxy)ethyl Phosphorylcholine

Bing Yu,[†] Andrew B. Lowe,*[,‡] and Kazuhiko Ishihara[§]

Department of Chemistry and Biochemistry, and School of Polymers and High Performance Materials, University of Southern Mississippi, 118 College Drive, No. 10076, Hattiesburg, Mississippi 39406, and Department of Materials Engineering, School of Engineering, The University of Tokyo, 7-3-1, Hongo, Bunkyo-ku, Tokyo 113-8656, Japan

Received December 23, 2008

Reversible addition-fragmentation chain transfer (RAFT) radical polymerization, mediated by 4-cyanopentanoic acid dithiobenzoate and 4,4′-azobis(4-cyanovaleric acid) (V-501) in water at 70 °C, of biocompatible 2-(methacryloyloxy)ethyl phosphorylcholine (MPC) yields a macro-chain transfer agent (CTA) that was employed in the synthesis of a range of stimulus-responsive AB diblock copolymers in protic media. Well-defined block copolymers of varying molar composition, with narrow molecular weight distributions ($M_w/M_n = 1.10-1.24$) were prepared with *N*,*N*-diethylacrylamide (DEAm), 4-vinylbenzoic acid (VBZ), *N*-(3-sulfopropyl)-*N*-methacryloyloxyethyl-*N*,*N*-dimethylammonium betaine (DMAPS), and the newly synthesized *N*,*N*-di-*n*-propylbenzylvinylamine (Dn-PBVA) in either methanol, 2,2,2-trifluoroethanol, or aqueous media. When a combination of ^{1}H NMR spectroscopy and dynamic light scattering is used, it is shown that all block copolymers are capable of existing as molecularly dissolved chains in aqueous media with average hydrodynamic diameters of ~6−7 nm provided the aqueous environment is appropriately tuned. Similarly, these unimers can be induced to undergo self-assembly in the same aqueous environment provided the correct external stimulus (change in temperature, pH, or electrolyte concentration) is applied. In such instances, aggregates with average sizes in the range of ~22−180 nm are formed and are most likely due to the formation of polymeric micelles and vesicles. Such self-assembly is also completely reversible. Removal, or reversal, of the applied stimulus results in the reorganization to the unimeric state.

Introduction

Polymeric betaines (polybetaines) are zwitterionic materials in which the cationic and anionic functional groups are located on the same monomer/repeat unit.[1,2] Such materials may be further differentiated based on the chemical nature of the negatively charged group and include the sulfo- (sulfonate),[3,4] carboxy- (carboxylate),[5−9] and phospho- (phosphonate)[10−17] betaines, as well as the less well-known dicyanoetheneolates.[18−22] Polybetaines were first reported in the 1950s[23,24] and since then have almost exclusively been prepared via the direct homogeneous aqueous solution radical polymerization of the corresponding betaine monomer. The preparation of well-defined polybetaines, as well as materials with more advanced architectures, has only been accomplished relatively recently. Lowe et al.[25−29] reported the group transfer polymerization synthesis of poly(2-(dimethylamino)ethyl methacrylate) (PDMAEMA) homopolymers as well as copolymers with various methacrylic comonomers of controlled molecular weight and low polydispersity that were modified postpolymerization by reaction of the tertiary amine residues in the DMAEMA residues with 1,3-propanesultone yielding the corresponding well-defined polysulfopropylbetaines. Such polymer analogous reactions are facile, selective, and essentially quantitative. The advent of controlled radical polymerization techniques has facilitated the direct (co)polymerization of sulfo-, carboxy-, and phosphobetaine monomers. For example, atom transfer radical polymerization has been employed extensively by Armes and co-workers in the preparation of a wide-range of materials based on the methacrylic phosphobetaine monomer 2-(methacryloyloxy)ethyl phosphorylcholine (MPC).[13,30−32] MPC is especially interesting given its well-documented biocompatibility.[11,12,33−40] Most recently, the direct[41] and indirect[42] synthesis of well-defined polysulfo- and polycarboxybetaines was accomplished by ring-opening metathesis polymerization (ROMP). Rankin and Lowe[41] described the rapid, direct, controlled homo- and copolymerization of *exo*-7-oxanorbornene sulfo- and carboxybetaine derivatives employing a novel 2,2,2-trifluoroethanol/CH_2Cl_2 solvent combination in conjunction with Grubbs first generation catalyst $RuCl_2(PCy_3)_2CHPh$. The only requirement for successful (co)polymerization was that the carboxybetaine be polymerized in the free acid form to prevent competitive complexation of carboxylate functional groups to the Ru metal center. Colak and Tew[42] disclosed the synthesis of oxa- and methylene bridged norbornene-based polycarboxybetaines employing protecting group chemistry. Polymerizations of ammonium monomers with *tert*-butyl ester groups were performed in THF/methanol at 60 °C employing the third generation Grubbs catalyst $RuCl_2PCy_3(3\text{-}BrPy)_2CHPh$. The free carboxybetaines were obtained postpolymerization by treatment with neat trifluoroacetic acid.

Reversible addition-fragmentation chain transfer (RAFT) radical polymerization[43−47] is, arguably, the most versatile of

* To whom correspondence should be addressed. E-mail: andrew.lowe@usm.edu.
[†] Department of Chemistry and Biochemistry, University of Southern Mississippi.
[‡] School of Polymers and High Performance Materials, University of Southern Mississippi.
[§] Department of Materials Engineering, The University of Tokyo.

10.1021/bm8014945 CCC: $40.75
Published on Web 02/25/2009

Table 1

entry	block copolymer	M_n expt	M_p expt[f]	M_w/M_n[f]	theoretical molar composition[g]	measured molar composition[h]
1	P(MPC-*b*-DEAm)[a]	12400	12900	1.10	80:20	82:18
2	P(MPC-*b*-DEAm)[a]	10700	12500	1.24	50:50	56:44
3	P(MPC-*b*-VBZ)[b]	10400	11100	1.10	80:20	89:11
4	P(MPC-*b*-VBZ)[b]	10200	11800	1.16	50:50	50:50
5	P(MPC-*b*-DnPBVA)[c]	11000	11700	1.18	50:50	70:30
6	P(MPC-*b*-DMAPS)[d]	12000	13300	1.13	70:30	76:24
7	P(MPC-*b*-DMAPS)[e]	12000	13500	1.17	50:50	58:42

[a] Polymerization conducted at 60 °C with thiocarbonylthio end-group/V-501 = 3:1 at a concentration of 25 wt % in MeOH. [b] Polymerization conducted at 80 °C with thiocarbonylthio end-group/V-501 = 3:1 at a concentration of 10 wt % in deionized water with 1 mol equiv of Na_2CO_3 based on VBZ to aid in the dissolution of the styrenic monomer. [c] Polymerization conducted at 70 °C with thiocarbonylthio end-group/V-501 = 3:1 at a concentration of 10 wt % in 2,2,2-trifluoroethanol. [d] Polymerization conducted at 60 °C with thiocarbonylthio end-group/V-501 = 3:1 at a concentration of 25 wt % in methanol. [e] Polymerization conducted at 80 °C with thiocarbonylthio end-group/V-501 = 3:1 at a concentration of 10 wt % in 0.25 M NaBr. [f] As determined by aqueous size exclusion chromatography, in 0.25 M NaBr, calibrated with narrow molecular mass poly(ethylene oxide) standards. [g] Assuming 100% conversion of the second block. [h] As determined by ^{1}H NMR spectroscopy.

the controlled radical polymerization techniques facilitating the controlled polymerization of the broadest range of monomer families. For example, aside from the common monomer families such as styrenics,[48−53] (meth)acrylates,[54,55] and (meth)acrylamides,[51−53,56−61] RAFT is suitable for nonactivated substrates such as vinyl esters,[62] vinyl amides,[62,63] and diallylammonium species.[64] RAFT has also been employed in the (co)polymerization of betaine monomers. The first report highlighting the application of RAFT in the synthesis of polybetaines was that of Laschewsky et al.[65] and was shortly followed by reports from Donovan and co-workers[66,67] who described the direct homopolymerization of styrenic, methacrylic, and acrylamido sulfopropylbetaine derivatives in aqueous media as well as AB diblock and ABA triblock copolymers with *N,N*-dimethylacrylamide. MPC has also been (co)polymerized by RAFT; Yusa et al.[68] described a detailed study of the synthesis and self-association of AB diblock copolymers of MPC with *n*-butyl methacrylate. In addition to MPC, Stenzel et al.[69] reported the RAFT polymerization of 2-(acryloyloxy-)ethyl phosphorylcholine and the ability to form biocompatible nanocontainers.

While MPC has been copolymerized via RAFT with a hydrophobic comonomer, this technique has not been utilized in the preparation of new water-soluble stimulus-responsive block copolymers. To address this, we describe herein the synthesis of a new pH-responsive monomer and the block copolymerization of MPC with a variety of stimulus-responsive, or "smart", neutral, ionic, and sulfobetaine comonomers. The comonomers were chosen to yield a range of materials exhibiting pH, temperature, or salt responsive properties that were anticipated to undergo reversible self-assembly in aqueous media as a function of such applied stimuli.

Experimental Section

All reagents were purchased from the Aldrich Chemical Co. at the highest available purity and used as received unless noted otherwise. *N,N*-Diethylacrylamide was purchased from Polysciences Inc. and purified by distillation. The sulfobetaine monomer, *N*-(3-sulfopropyl)-*N*-methacrylooxyethyl-*N,N*-dimethylammonium betaine (DMAPS), was prepared from the reaction between 2-(dimethylamino)ethyl methacrylate and 1,3-propanesultone in THF at ambient temperature.[25] 4-Cyanopentanoic acid dithiobenzoate,[70] 2-(methacryloyloxy)ethyl phosphorylcholine,[10] and 4-vinylbenzoic acid[70] were prepared according to literature procedures. 4,4′-Azobis(4-cyanovaleric acid) (V-501) was purified by recrystallization from MeOH and stored at −20 °C until needed.

Synthesis of *N,N*-Di-*n*-propyl-4-vinylbenzylamine (DnPBVA). A mixture of 4-vinylbenzyl chloride (29.54 g, 0.194 mol), di-*n*-propylamine amine (50.0 g, 0.387 mol), methanol (50.0 mL, HPLC grade), and a small amount of phenothiazine were added to a 500 mL round-bottom flask equipped with a magnetic stirring bar and a western condenser. The solution was then refluxed for 14 h. Subsequently, methanol was removed using a rotary evaporator. The residue was then dissolved in 4.0 M HCl (100 mL), and this solution was washed three times with diethyl ether (3 × 100 mL). NaOH was then added to the aqueous phase until the solution became slightly basic, after which it was washed three times with diethyl ether (3 × 100 mL). The ether washings were combined and the solvent was removed using a rotary evaporator to give a crude product yield of 76%. The target monomer was purified via fractional distillation (bp of ~80 °C at ~1 mbar).

Homopolymerization of 2-(Methacryloyloxy)ethyl Phosphorylcholine (MPC). To a Schlenk flask, equipped with a magnetic stir bar were added MPC (3.0 g, 10.2 mmol), 4-cyanopentanoic acid dithiobenzoate (CTP; 28 mg, 0.10 mmol), V-501 (5.6 mg, 2.0×10^{-2} mmol), deionized H_2O (15.0 g), and 5 wt % $NaHCO_3$ solution (336 mg). The mixture was then stirred for at least 4 h in an ice-bath to ensure complete dissolution of CTP and V-501. The solution was then purged with nitrogen prior to immersion in a preheated oil-bath at 70 °C. After 2 h, the polymerization was stopped via rapid cooling and exposure to air. The polymerization solution was then dialyzed against deionized water for 12 h with 3 changes of the deionized water. Homopolymer was then recovered by freeze-drying, yielding 1.7 g of material (yield of 56.7%).

Synthesis of Poly(MPC-block-4-vinylbenzoic acid), 50:50. All AB diblock copolymers were prepared using the same general approach. Any differences in reaction medium or polymerization temperature are noted in Table 1. Below is detailed the synthesis of a poly(MPC-*block*-4-vinylbenzoic acid) with a target molar composition of 50:50 as a representative example.

A mixture of polyMPC (0.5 g, equivalent to 1.69 mmol of MPC repeat units), 4-vinylbenzoic acid (VBZ; 0.251 g, 1.69 mmol), V-501 (2.8 mg, 9.93×10^{-3} mmol), Na_2CO_3 (180 mg, 1.70 mmol), and deionized H_2O (6.8 g) were added to a Schlenk flask equipped with a magnetic stir bar. The mixture was then stirred for at least 4 h in an ice-bath to ensure complete dissolution of V-501 and VBZ. The solution was then purged with nitrogen prior to immersion in a preheated oil-bath at 80 °C for 12 h. The polymerization was stopped by rapid cooling and exposure to air. The copolymer solution was then was dialyzed against deionized H_2O for 6 h with three changes of the deionized water. The polymer was recovered by freeze-drying.

Sample Preparation for Dynamic Light Scattering Experiments. Samples for dynamic light scattering were prepared as follows: 1.0 wt % solutions were prepared in 5 mL scintillation vials using the appropriate aqueous solution. The solution was then filtered through a Millex syringe filter with a pore size of 0.45 μm and 0.35 mL of the filtered solution was transferred to a polystyrene cuvette using a Rainin P1000 micro Pipette.

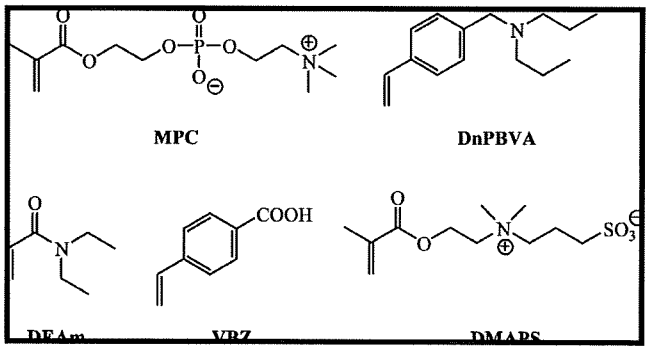

Figure 1. Chemical structures of monomers used in this study.

General Instrumentation. ^{1}H (300 MHz) NMR and ^{13}C (75 MHz) NMR spectra were recorded on a Bruker 300 53 nm spectrometer in appropriate deuterated solvents or solvent mixtures. Aqueous size exclusion chromatography experiments were conducted on a Viscotek system comprised of a Viscotek VE1122 pump, Viscotek VE3580 RI detector, a Viscotek viscoGEL PW_{XL} guard column followed by a series of two viscoGEL columns (G5000PW_{XL} +G4000 PW_{XL}), in 0.25 M NaBr solution, which was degassed prior to use at a flow rate of 1.0 mL/min. The columns were calibrated with a series of narrow molecular weight distribution PEO/PEG standards. Data was manipulated using the Omnisec V4.1 software. Dynamic light scattering (DLS) experiments were conducted on a Malvern Instruments Zetasizer Nano-ZS (red badge) instrument operating with a 633 nm laser. Data was collected and processed with the Dispersion Technology software V5.10.

Results and Discussion

With the aim of preparing and examining a range of new water-soluble, stimulus-responsive block copolymers based on the biocompatible building block 2-(methacryloyloxy)ethyl phosphorylcholine (MPC), a new pH-responsive styrenic monomer was initially prepared, Figure 1. *N,N-n*-Propyl-4-vinylbenzylamine (DnPBVA) was prepared in a straightforward manner from the reaction between 4-vinylbenzylchloride and di-*n*-propylamine and isolated in good yield. The structure of the product was confirmed via a combination of ^{1}H/^{13}C NMR and FTIR spectroscopies. Figure 2 shows the ^{1}H (a) and ^{13}C (b) NMR spectra of DnPBVA, recorded in $CDCl_3$, with peak assignments, verifying structure and purity.

With the exception of *N,N*-diethylacrylamide (DEAm), all other monomers were prepared according to established literature procedures. With all monomers in hand, a polyMPC (PMPC) homopolymer was prepared according to the method of Yusa et al.,[68] Scheme 1.

Homopolymerization of MPC was conducted in water for 2 h at 70 °C using the CTP/V-501 RAFT chain transfer agent (CTA)/initiator combination, with a target M_n of 30000 at quantitative conversion. The resulting MPC homopolymer was purified by dialysis against deionized water for 12 h and subsequently analyzed via a combination of NMR spectroscopy and aqueous size exclusion chromatography (ASEC).

Figure 3a shows the ASEC trace of the purified MPC homopolymer. The chromatogram is unimodal and symmetric, and the homopolymer has an experimentally determined M_n, relative to narrow molecular weight poly(ethylene oxide) standards of 12100, with a corresponding polydispersity index (M_w/M_n) of 1.12. Figure 3b shows the ^{1}H NMR spectrum, recorded in D_2O, of the same MPC homopolymer. Importantly, the resonances associated with the phenyl group of the dithioester end-group are visible and therefore facilitates the determination of the absolute molecular weight. Assuming one phenyl group per polymer chain, a comparison of the integral associated with the phenyl hydrogens with those labeled c yields a calculated absolute M_n of 25400.

Having verified the ability to prepare PMPC in a controlled manner directly in aqueous media, AB diblock copolymers of varying molar composition were prepared with a range of comonomers from different monomer families with different aqueous solution characteristics. For example, homopolymers prepared from DEAm are readily soluble in water at ambient temperature but possess a lower critical solution temperature (LCST) of about 32 °C, essentially identical to the more commonly studied poly(*N*-isopropylacrylamide). Homopolymers derived from VBZ are pH-responsive. Specifically, when ionized, that is, at intermediate-to-high solution pH, homopolymers of VBZ are readily water-soluble. However, in the free acid form, at low pH, such materials undergo a distinct hydrophilic-to-hydrophobic phase transition and become insoluble. We, and others, have previously taken advantage of this pH-trigger in the synthesis of copolymers capable of undergoing pH-induced reversible self-assembly.[50,51,70,71] Homopolymers of DnPBVA likewise exhibit pH-dependent solubility characteristics, although it is opposite to that exhibited by materials containing VBZ, that is, such materials are hydrophilic at low pH when the amine resides are protonated but become hydrophobic when deprotonated. Such behavior is entirely consistent with the structurally similar monomer *N,N*-dimethylvinylbenzylamine.[70] Finally, homopolymers derived from the sulfobetaine monomer DMAPS possess electrolyte responsive features in water.[2,28] Generally, polymeric betaines exhibit limited-to-zero solubility in pure water due to the formation of an ionically cross-linked network-like structure. The addition of a small molecule electrolyte, such as NaCl, at some critical concentration effectively screens these ionic interactions resulting in dissolution. Once in solution, the addition of further salt results in a second, less pronounced conformational effect. In contrast to polyelectrolytes, which undergo chain contraction with added electrolyte, polymeric betaines undergo chain expansion, a phenomena referred to as the *antipolyelectrolyte effect*.[1] With respect to DMAPS, it is the former, more pronounced, effect that is of interest.

Table 1 gives a summary of the AB diblock copolymers that were prepared, their targeted and measured molar compositions, and M_n and polydispersity indices. Several points are worth highlighting. The varied, and sensitive, aqueous solution behavior of the target comonomers/polymers requires careful identification of suitable conditions for effective block copolymerization. The polymerization conditions noted were those found to give acceptable control/kinetics, conversions, and low PDIs. In all instances, V-501 was used as the source of primary radicals at a ratio of 3:1 thiocarbonylthio end-group/initiator. In the case of block copolymers with DEAm, Table 1, entries 1 and 2, copolymerizations were performed at 60 °C in MeOH at a total concentration of 25 wt %. In fact, MeOH is a convenient solvent for MPC and its copolymers and is commonly employed in ATRP syntheses.[30,31,72] DEAm can also be copolymerized in water although this requires a low temperature initiator since, as noted above, PDEAm has an LCST of about 32 °C. Similar polymerization conditions were used for one of the block copolymers with DMAPS, Table 1, entry 6, thus negating the need for added electrolyte in the case of aqueous based polymerization although this is also a feasible approach, Table 1, entry 7. In the case of VBZ block copolymers, Table 1, entries 3 and 4, syntheses were performed in water under

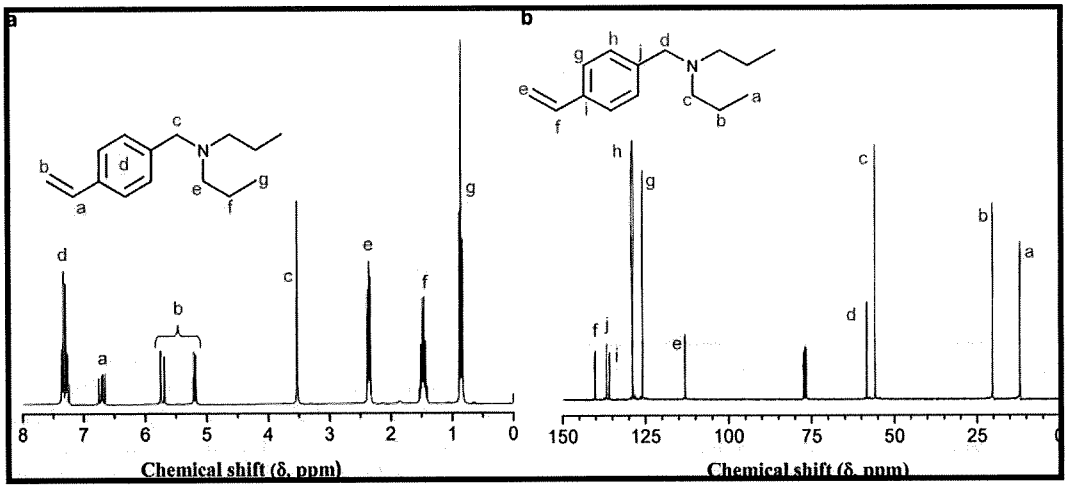

Figure 2. ^{1}H (a) and ^{13}C (b) NMR spectra, recorded in $CDCl_3$, of *N,N*-di-*n*-propylbenzylvinylamine.

Scheme 1. Synthetic Outline for the Preparation of a PMPC Macro-CTA

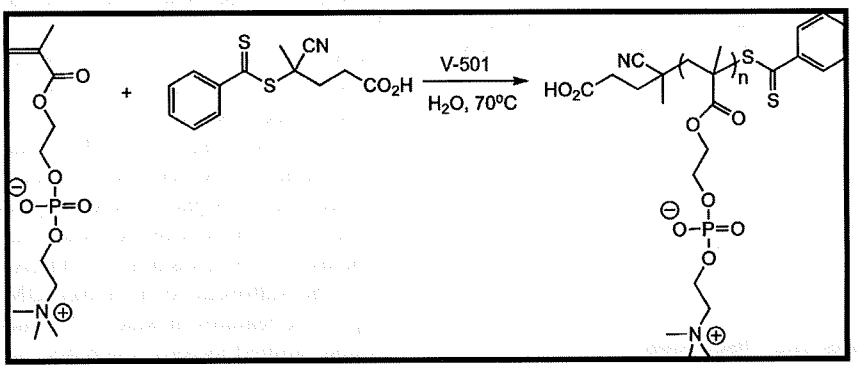

slightly basic conditions although at a lower concentration of 10 wt % and slightly higher reaction temperature of 80 °C. In the case of the block copolymer with DnPBVA, Table 1, entry 5, copolymerization proceeded smoothly in 2,2,2-trifluoroethanol (TFE) at a concentration of 10 wt % and 70 °C. While these synthetic conditions are varied, each of the resulting block copolymers presents a symmetric, unimodal ASEC trace with the final polydispersity indices in the range 1.10−1.24. As representative examples, Figure 4 shows the ASEC traces for the MPC-*b*-DEAm, Table 1, entry 1, and MPC-*b*-DMAPS, Table 1, entry 7, copolymers.

With a series of PMPC-based AB diblock copolymers in hand the aqueous solution properties of specific samples were briefly examined using a combination of ^{1}H NMR spectroscopy and dynamic light scattering (DLS). NMR is particularly useful for monitoring the change in solvation of a particular block under different solution conditions, while DLS is a fast and convenient method for measuring the hydrodynamic properties of copolymers, and aggregates thereof. Figure 5a shows the ^{1}H NMR spectra of the P(MPC-*b*-DEAm) copolymer with a molar composition of 56:44, Table 1, entry 2, at ambient temperature. All the resonances associated with the MPC and DEAm blocks are clearly present. With respect to the DEAm block, the major resonances are those labeled d, e, and f and are associated with the backbone hydrogens, the aza-methylene group, and the methyl hydrogens, respectively. Heating the P(MPC_{56}-*b*-$DEAm_{44}$) copolymer solution in the NMR spectrometer to 50 °C results in an NMR spectrum, Figure 5b, devoid of any signals associated with the DEAm block. Specifically, there are three distinct changes. First, the signals labeled d and e in Figure 5a are completely absent, while there is also a significant decrease in the intensity of the signal at $\delta \sim 1.1$ ppm. These changes are completely consistent with desolvation of the DEAm block. Because there is no evidence of macroscopic precipitation and given the block architecture of the material, such changes are entirely consistent with a self-assembly process yielding, for example, spherical polymeric micelles, Scheme 2. The formation of aggregate structures under these conditions was verified by dynamic light scattering (DLS). Figure 5c shows the measured size distributions for a 1 wt % aqueous solution (0.1 M NaCl) of the P(MPC_{56}-*b*-$DEAm_{44}$) copolymer employed in the NMR study at 22 and 50 °C. At the lower temperature DLS indicates an average hydrodynamic diameter (D_h) of ~6.0 nm, which is entirely consistent with molecularly dissolved polymer chains (unimers) of the measured average molecular weight. In contrast, after heating the solution to 50 °C the size distribution shifts significantly indicating the presence of a species with an average D_h of ~180 nm. Such a dramatic change in the D_h certainly indicates that the AB diblock copolymer is undergoing self-assembly forming an aggregate structure such as a micelle, vesicle, or higher ordered structure. We have not, at this time, attempted to elucidate the exact nature of the aggregate species. However, such assembly is completely reversible. Cooling the solution back down to room temperature results in the disappearance of the large aggregates and the reappearance of the smaller, unimer population. Similarly, temperature cycling in the NMR spectrometer confirms the reversible solvation-desolvation of the DEAm residues (data not shown).

Figures 6−8 show the results from the same series of experiments for the P(MPC_{50}-*b*-VBZ_{50}), P(MPC_{70}-*b*-DnPB-VA_{30}), and the P(MPC_{76}-*b*-$DMAPS_{24}$) copolymers, Table 1, entries 4−6.

Consider first the P(MPC_{50}-*b*-VBZ_{50}) copolymer. Figure 6a shows the ^{1}H NMR spectrum of the block copolymer under

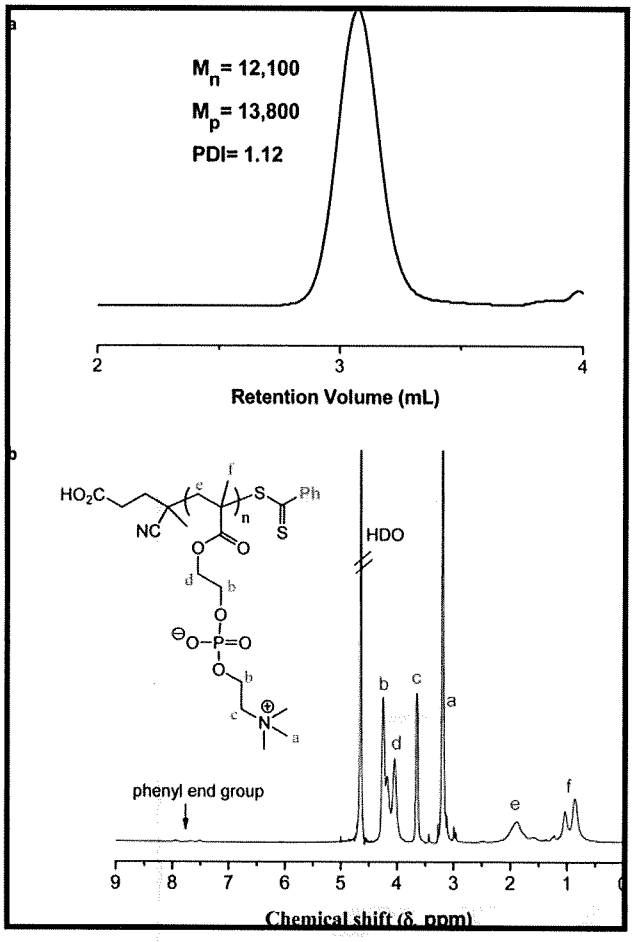

Figure 3. Aqueous size exclusion chromatogram (a; RI signal) of a PMPC homopolymer, and the ^{1}H NMR spectrum (b) of the same homopolymer recorded in D_2O, with peak assignments.

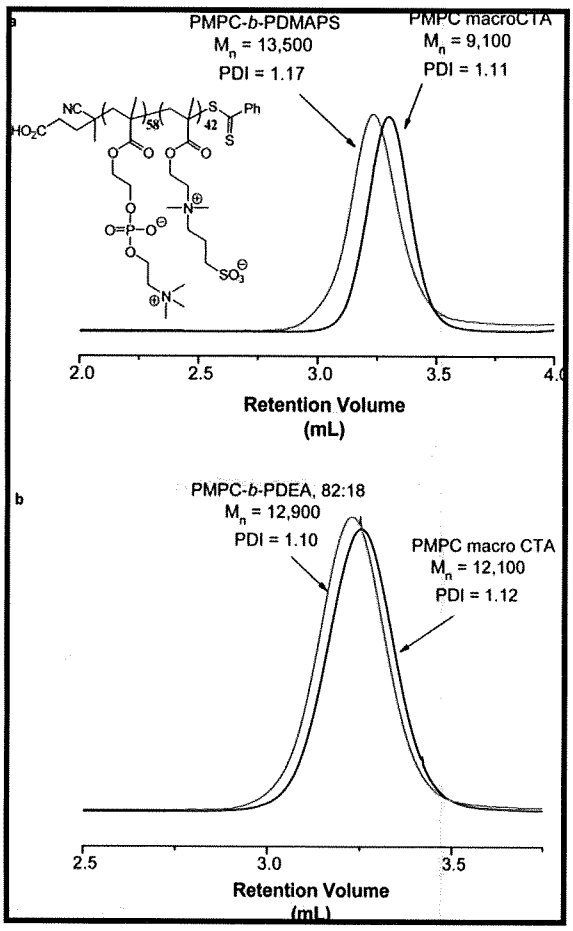

Figure 4. Aqueous size exclusion chromatograms (RI signal) of examples of PMPC-based AB diblock copolymers, P(MPC_{58}-*b*-$DMAPS_{42}$) (a) and P(MPC_{82}-*b*-$DEAm_{18}$) (b), demonstrating successful block copolymer formation.

conditions in which both the MPC and the VBZ blocks are hydrophilic and thus solvated, that is, under basic solution conditions in which the VBZ block is ionized. The key signals associated with MPC are again clearly visible as well as the key resonance for the VBZ block, the two signals spanning $\sim\delta = 6-7.5$ ppm, associated with the four hydrogens of the benzene ring. Acidification of this solution with DCl results in spectrum Figure 6b. The signals associated with MPC are still present but those associated with VBZ are absent. As with the temperature-induced desolvation observed for the P(MPC_{56}-*b*-$DEAm_{44}$) copolymer, this pH-induced change also leads to the formation of nanosized aggregates as evidenced by DLS. Figure 6c shows the measured DLS size distributions for the MPC-*b*-VBZ block copolymer at a concentration of 1 wt %, 22 °C, in 0.2 M NaOH and 0.2 M HCl. Under basic conditions, when both blocks are hydrophilic, DLS indicates the presence of unimers with an average D_h of ~7.0 nm. However, under acidic conditions a rather broad size distribution comparable to that observed for the P(MPC_{56}-*b*-$DEAm_{44}$) copolymer is seen with an average D_h of ~124 nm and a corresponding polydispersity of 0.25. Again, such a size may indicate the presence of vesicles or higher ordered structures as opposed to spherical micelle-like species. Given the similar block copolymer compositions and molecular weights of these P(MPC_{56}-*b*-$DEAm_{44}$) and P(MPC_{50}-*b*-VBZ_{50}) copolymers, it is perhaps not surprising that they behave similarly in their amphiphilic forms even though such behavior is induced by a different external stimulus. The P(MPC_{70}-*b*-$DnPBVA_{30}$) copolymer also exhibits pH-induced self-assembly characteristics although the pH-trigger is reversed.

As noted above, the DnPBVA residues are hydrophilic at low pH but hydrophobic at intermediate-to-high pH. Figure 7a shows the ^{1}H NMR spectrum of the P(MPC_{70}-*b*-$DnPBVA_{30}$) under acidic conditions where both blocks are hydrophilic and solvated. The main, identifiable, signals associated with the DnPBVA block are those associated with the aromatic ring at $\sim\delta = 6-7.2$ ppm as well as the signal at $\sim\delta = 2.7$ ppm. Under basic conditions, both of these key signals disappear consistent with the pH-induced hydrophilic−hydrophobic transition of the DnPBVA residues. DLS again confirms the occurrence of a self-assembly process with this change in solution pH. For a 1 wt % solution of the P(MPC_{70}-*b*-$DnPBVA_{30}$) at 22 °C, a unimers distribution with an average D_h of ~6 nm is observed. Deprotonation of the DnPBVA residues renders them hydrophobic and self-assembly occurs yielding aggregates with a D_h of ~22 nm. This size is much smaller than those observed for either the P(MPC_{56}-*b*-$DEAm_{44}$) or P(MPC_{50}-*b*-VBZ_{50}) copolymers, although it must be noted that the copolymer composition is significantly different. Finally, the P(MPC_{76}-*b*-$DMAPS_{24}$) copolymer was examined with respect to the effect of electrolyte on solubility/self-assembly. In the case of the NMR experiments, little or no change was observed in peak intensities when spectra were recorded in the presence and absence of electrolyte indicating that the DMAPS block was still in a solvated, although perhaps somewhat reduced, state. In contrast, DLS experiments did indicate the presence of aggregate structures for the block copolymer in deionized water. Figure 8 shows

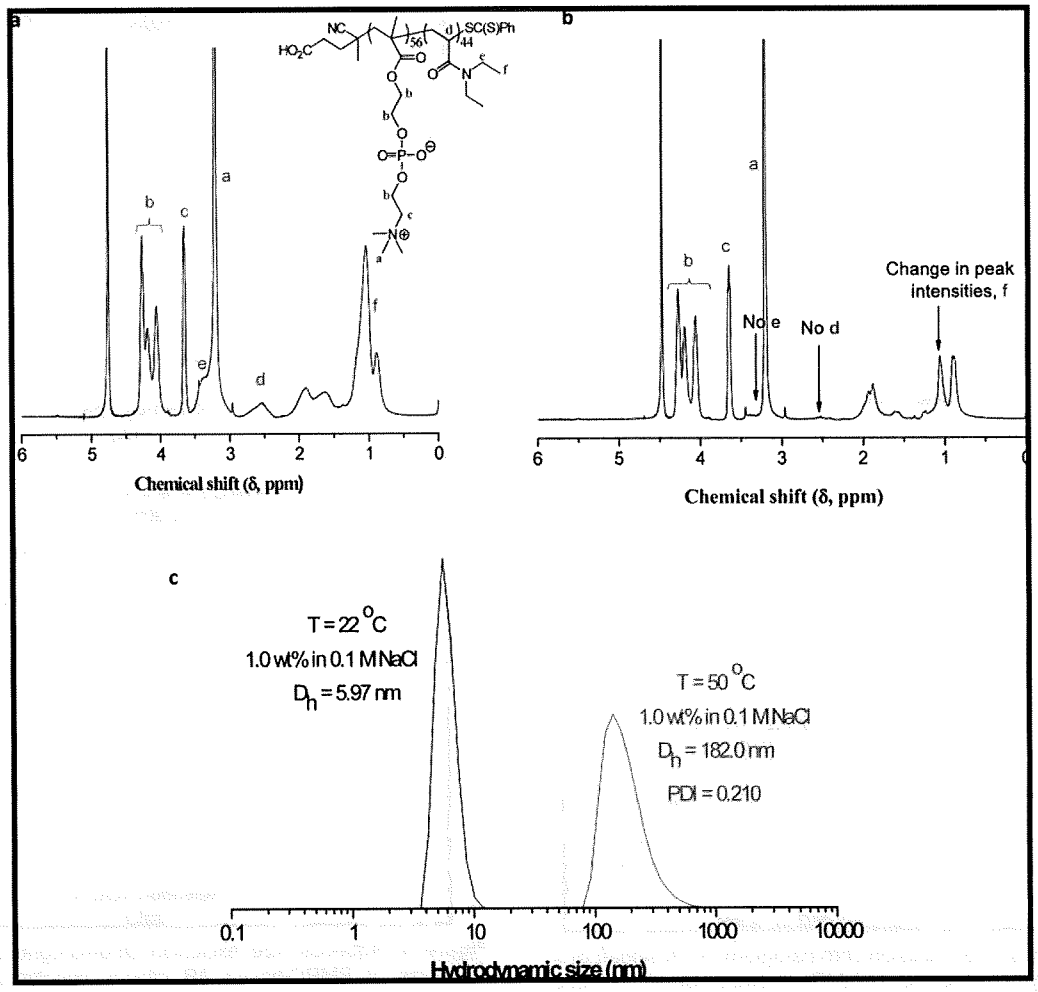

Figure 5. ^{1}H NMR spectra, recorded in D_2O, of the P(MPC_{56}-*b*-$DEAm_{44}$) at ambient temperature (a) and at 50 °C (b) demonstrating the desolvation of the DEAm block as a function of change in solution temperature and the intensity-average size distributions measured by dynamic light scattering (c) as a function of temperature highlighting the formation of aggregates.

Scheme 2. Idealized, Reversible Self-Assembly, with the Possible Formation of Either Micelles or Vesicles, of "Smart" AB Diblock Copolymers Based on PMPC

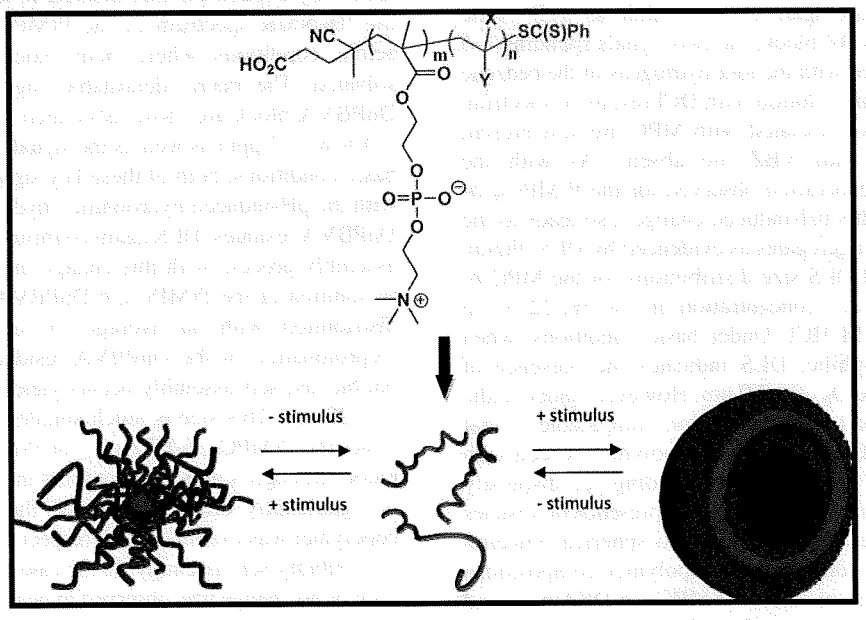

the measured size distributions for the P(MPC_{76}-*b*-$DMAPS_{24}$) copolymer in 0.5 M NaCl and deionized water at a concentration of 1 wt % at 22 °C. In the electrolyte solution unimers are observed with an average D_h of ~6 nm. In contrast, when dissolved directly in deionized water aggregates are observed with an average D_h of 174 nm. A more detailed, fundamental study of the effect of block copolymer composition on the self-assembly properties of these copolymers is currently underway.

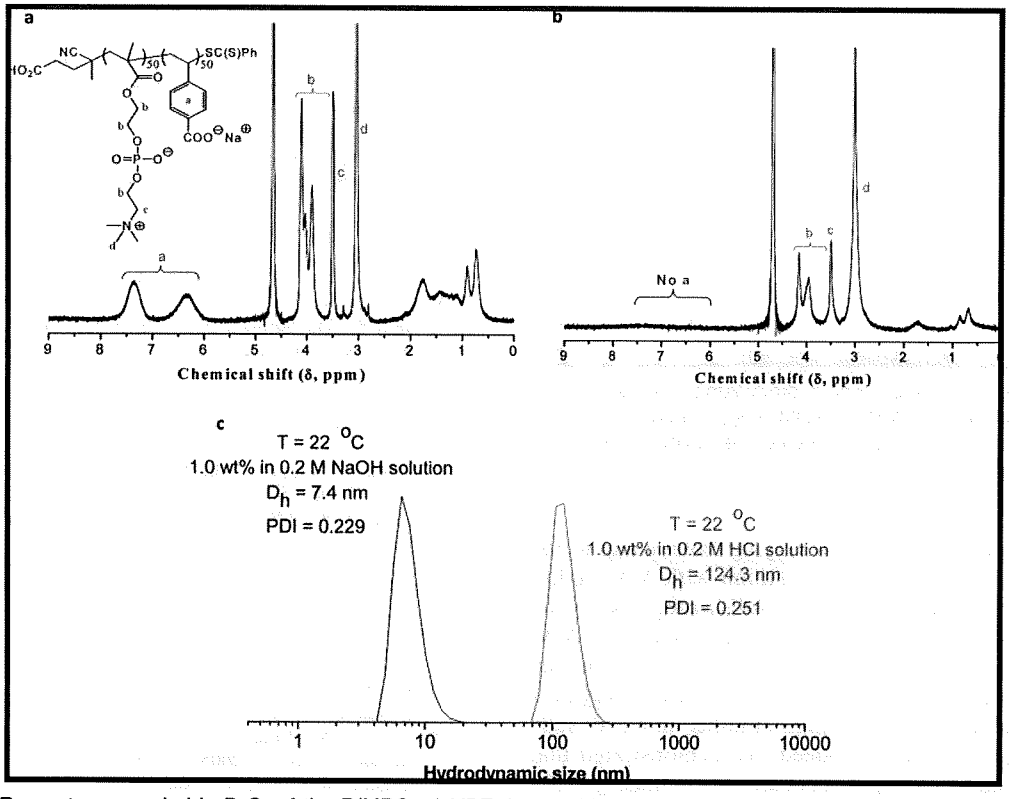

Figure 6. ^{1}H NMR spectra, recorded in D_2O, of the P(MPC_{50}-*b*-VBZ_{50}) at ambient temperature under basic conditions (a) and under acidic conditions (b), demonstrating the desolvation of the VBZ block as a function of change in solution pH and the intensity-average size distributions measured by dynamic light scattering (c) as a function of pH highlighting the formation of aggregates.

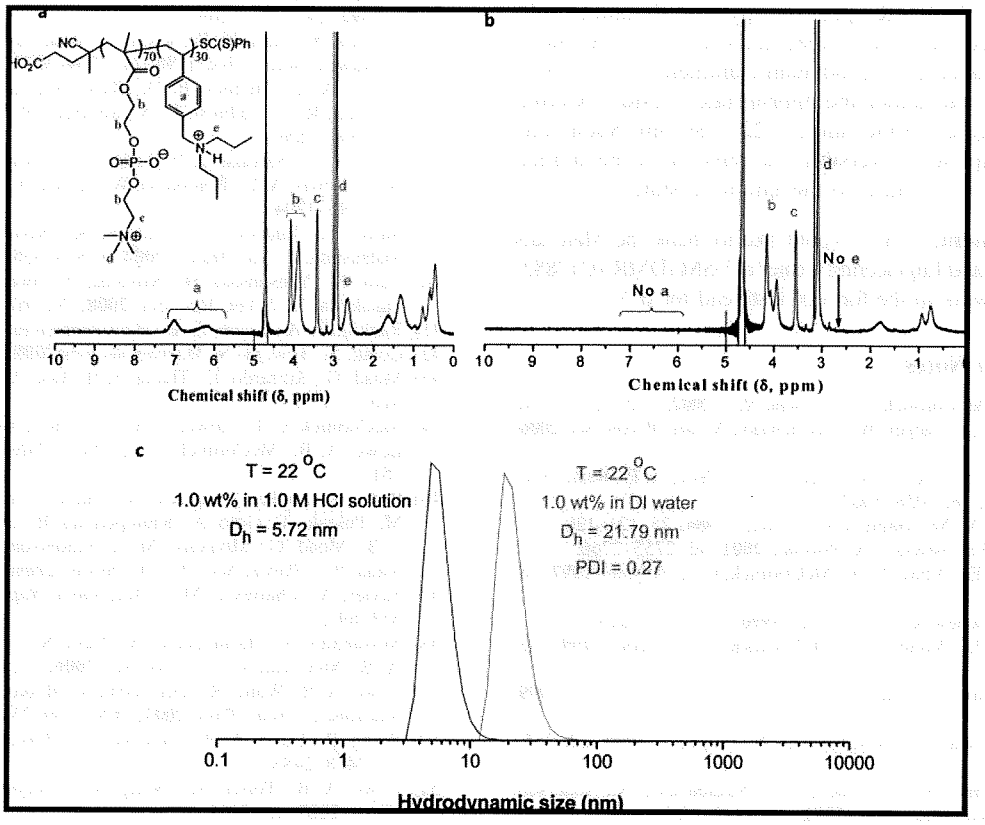

Figure 7. ^{1}H NMR spectra, recorded in D_2O, of the P(MPC_{70}-*b*-$DnPBVA_{30}$) at ambient temperature under acidic conditions (a) and under neutral/basic conditions (b), demonstrating the desolvation of the DnPBVA block as a function of change in solution pH and the intensity-average size distributions measured by dynamic light scattering (c) as a function of pH highlighting the formation of aggregates.

Summary and Conclusions

We have demonstrated herein that reversible addition-fragmentation chain transfer (RAFT) radical polymerization is a convenient method for the synthesis of a range of AB diblock copolymers based on the PMPC with a range of "smart" comonomers. Employing a MPC macro-CTA, well-